





OPEN ACCESS

Original research

Microbiota fasting-related changes ameliorate cognitive decline in obesity and boost ex vivo microglial function through the gut-brain axis

Virginia Mela ^{1,2,3} Violeta Heras^{1,2,3} Monika Ilesmantaite^{1,4}
 María Luisa García-Martín^{5,6,7} Manuel Bernal ^{8,9,10} Joel D Posligua-García^{8,9}
 Alba Subiri-Verdugo^{1,2,3,11} José Ignacio Martínez-Montoro^{1,2,3,11}
 Ana María Gómez-Pérez^{1,2,3,11} Borja Bandera^{1,2,3,11} Isabel Moreno-Indias^{1,2,3}
 Francisco J Tinahones^{1,2,3,11}

► Additional supplemental material is published online only. To view, please visit the journal online (<https://doi.org/10.1136/gutjnl-2025-335353>).

For numbered affiliations see end of article.

Correspondence to

Dr Virginia Mela;
virginiamelaras@gmail.com

VH and MI contributed equally.

IM-I and FJT are joint senior authors.

Received 17 March 2025
 Accepted 25 April 2025



© Author(s) (or their employer(s)) 2025. Re-use permitted under CC BY-NC. No commercial re-use. See rights and permissions. Published by BMJ Group.

To cite: Mela V, Heras V, Ilesmantaite M, *et al.* Gut Epub ahead of print: [please include Day Month Year]. doi:10.1136/gutjnl-2025-335353

ABSTRACT

Background Obesity-related cognitive decline is linked to gut microbiota dysbiosis, with emerging evidence suggesting that dietary interventions may ameliorate cognitive impairment via gut-brain axis modulation. The role of microglial cells in this process remains underexplored.

Objective To investigate how diet-induced changes in gut microbiota influence cognitive function in individuals with obesity and their microglial activity, and to determine the impact of specific dietary interventions.

Design This study included 96 participants with obesity who were randomised into three dietary intervention groups: Mediterranean diet (Med), alternate-day fasting (ADF) and ketogenic diet (Keto). Cognitive performance and microbiota composition were assessed pre-intervention and post-intervention. The effects of microbiota-related changes on microglial function were further evaluated in mice models through faecal transplantation and in vitro model with microbiota exosome treatment.

Results Both the Keto and ADF groups demonstrated significant weight loss, but cognitive performance improved most notably in the ADF group, in association with reduced inflammation. Diet-related microbiota composition was correlated with the cognitive outcomes in the human study. Mice models confirmed that the cognitive benefits of ADF were microbiota-dependent and linked to enhanced microglial phagocytic capacity and reduced inflammation, accompanied by changes in microglia morphology.

Conclusion Fasting-induced modifications in gut microbiota contribute to cognitive improvement in individuals with obesity, with microglial cells playing a crucial mediatory role. Among the interventions, ADF most effectively enhanced microglial function and cognitive performance, suggesting its potential as a therapeutic strategy for obesity-related cognitive decline. Further studies are required to fully elucidate the underlying mechanisms.

Trial registration number NCT04453150.

WHAT IS ALREADY KNOWN ON THIS TOPIC

⇒ Obesity is associated with cognitive decline, often linked to low-grade systemic inflammation, affecting gut microbiota, which impacts brain function through the gut-brain axis.

WHAT THIS STUDY ADDS

⇒ This study reveals that fasting-induced changes in gut microbiota significantly improve cognitive function in individuals with obesity, with microglial cells playing a crucial role in this process.

HOW THIS STUDY MIGHT AFFECT RESEARCH, PRACTICE OR POLICY

⇒ These findings could influence future research directions and clinical practices in dietary management for targeting gut microbiota as a viable strategy to prevent or mitigate cognitive decline.

INTRODUCTION

It is well known that obesity is accompanied by cognitive impairment, which could increase the risk of developing neurodegenerative disease.¹ In the last decade, the number of studies about obesity and age-related diseases has significantly increased. Due to the close interconnection between endocrine, immune and central nervous systems, obesity and ageing share common underlying complications. It has become clear that both processes share one common player, 'the low-chronic inflammation state',^{2,3} which is triggered by obesity-related dystrophic adipocytes in white adipose tissue (WAT)^{4,5} or by the so-called 'inflamm-ageing' process related to the cellular senescence in the aged body.⁶ However, few studies have tried to elucidate the interplay between the senescent process and obesity development. The obesity process is associated with increased adipocyte size, leading to inflammation due to the activation of the resident macrophage population within the WAT.⁷ It has been demonstrated how

this inflammation process can spread and affect other systems in the body, including the brain.⁸ Interestingly, the brain also hosts a resident population of immune cells called microglia, whose principal role is to protect neurons. Microglial cells share functions with the macrophages,⁹ and it has been shown that they become progressively dysfunctional with age-associated low-grade inflammation, which may accelerate the neurodegenerative process.¹⁰ The shared functions between these two cell types suggest a pivotal role for microglial cells in the progression from obesity to age-related changes in the brain. Due to the strong link between these cells, strategies focused on decreasing WAT mass might also affect the brain's immune system, counteracting the obesity-related inflamm-ageing. Among the different lifestyle strategies, a low-calorie diet intervention, particularly based on a Mediterranean (Med) diet, has been the most recommended by endocrinologists to reduce weight and WAT mass. In the social media era, new dietary programmes, such as restrictive diets or fasting patterns, have been gaining popularity, encouraging specialists to consider them for their dietary programmes and study their benefits compared with the classical ones.¹¹ It is well known that the increase in lipolysis during a negative energy balance is associated with an increase in the concentration of ketone bodies produced by the liver from the oxidation of fatty acids.¹² Indeed, the most popular diets lately are the ones based on increasing ketone bodies, such as the ketogenic (Keto) diet or diet based on fasting. Ketone bodies serve as cell fuel even more efficiently than glucose,¹³ bringing a positive effect on brain cognitive functions in situations of glucose scarcity.¹⁴ In addition, emerging evidence suggests that ketone bodies, such as β -hydroxybutyrate (BHB) and acetoacetate, could influence microglial function through its anti-inflammatory effects, providing cognitive protection and synaptic support in neurodegenerative diseases.^{15,16} Although ketone bodies can enter the brain through the monocarboxylate transporters at the blood-brain barrier (BBB), another intermediate may be responsible for their cognitive benefits. Interestingly, a bidirectional effect between gut microbiota and ketone bodies has been shown. On the one hand, ketone body metabolism is regulated by fasting-related changes in gut microbiota.¹⁷ On the other hand, gut microbiota composition is modified by diet based on ketone bodies, showing, among other changes, a depletion of *Bifidobacteria*^{17,18} associated with a lower inflammatory state in obesity. Considering that inflammation during obesity has been associated with a higher risk of neurodegenerative process,¹⁹ it is not surprising that the increase in ketone bodies through the Keto diet and/or fasting patterns could protect against the cognitive decline occurring in Alzheimer's disease (AD) by altering brain metabolism through gut microbiota modifications.^{20,21} The so-called 'microbiota-gut-brain axis' (GMBA) describes the bidirectional communication between both organs through the immune activation by microbial metabolites and peptides release and the *vagus* nerve activation by gut neurotransmitters and neuromodulator production. Obesity can affect the BBB integrity, increasing its permeability,²² so maintaining gut microbiome and BBB integrity through dietary interventions could be crucial for preventing neurological disorders and other brain alterations. When the BBB is damaged, microglial cells become a key player to protect the brain by controlling its homeostasis. However, these cells become overactivated due to obesity-related chronic inflammation²³ losing their functions, leading to a worse scenario which could accelerate brain ageing.

Although there are clues in the literature about how this GMBA could work in obesity-related cognitive impairment,²⁴ some pieces from this puzzle are still missed. Therefore, the present

manuscript aims to understand the critical role of microglial cells in gut-brain axis communication. Specifically, how microglial cells could mediate the effect of microbiota composition in the cognitive performance of the individual suffering from obesity and how microbiota diet-related changes could be used to alleviate obesity cognitive impairment.

MATERIALS AND METHODS

Human subjects

A total number of 96 healthy participants with obesity from both sexes (68% women; 32% men) enrolled in this study (32 per group, aged between 18 and 65 years and body mass index (BMI) between 30 and 45 kg/m²), which was recruited from the outpatient clinics of the Endocrinology and Nutrition Department at Virgen de la Victoria University Hospital in Malaga. Exclusion criteria: pregnancy or breastfeeding period; being recently diagnosed with coeliac, Crohn's or any disease, which could alter the nutritional status, allergies or food intolerances as well as being treated with antibiotics and/or probiotics. This is a substudy from the one registered at ClinicalTrials.gov (NCT04453150). By the end of the intervention, 26 in the Med group, 28 in the Keto group and 30 in the alternate-day fasting (ADF) group completed the full 3-month protocol. Thus, the dropout rates were 18.75% for Med, 12.5% for Keto and 6.25% for ADF, suggesting higher adherence in the ADF group (see figure 1 for experimental design and dropout rates details).

Human dietary interventions

The participants were subjected to a 3-month dietary intervention randomly assigned in a 1:1:1 ratio to three types of hypocaloric diets, which differ in ketone bodies source and concentrations: Med diet (low ketone bodies increase from the diet), ADF (high ketone bodies increase from the fasting pattern) and Keto diet (high ketone bodies increase from the diet), respectively. Randomisation was performed using a parallel-group design with individual-level allocation conducted by an independent researcher who was not involved in the data collection or analysis. Assignments were generated using a computerised random-number generator tool (www.random.org), ensuring unbiased allocation to each dietary group. No stratification was applied, and randomisation sequences were concealed until the point of assignment to minimise allocation bias. The composition of those diets is detailed below, and its caloric deficit was calculated according to the Harris-Benedict equation (1919) in a personal manner. Moreover, a daily physical activity programme was recommended for all participants, which included 250 min/week of fasting walk and/or strength training as a minimum goal.

1. Med diet was performed with a 600 kcal/day caloric deficit and the following caloric distribution: 45% carbohydrates, 35% fat and 20% protein. Med dietary pattern is based on olive oil as the main fat source; regular vegetables (two servings/day), fruits (three servings/day), legumes (three servings/week) and fish (three servings/week) intake; red meat/sausages reduced intake (less than two times/week) and dairy products, sugary drinks and factory-made pastries limited intake (less than one time/week). This dietary programme was recommended as, at least, four meals/day (breakfast, lunch, evening snack and dinner).
2. ADF was based on a 24-hour fast-24-hour feed cycle. During 'feed day', a normo-caloric diet is followed, while 'fast day' involves only 25% of the caloric needs (400–800 kcal) with the following caloric distribution: 5% carbohydrates, 65% fats and 30% proteins of high biological value. The intake

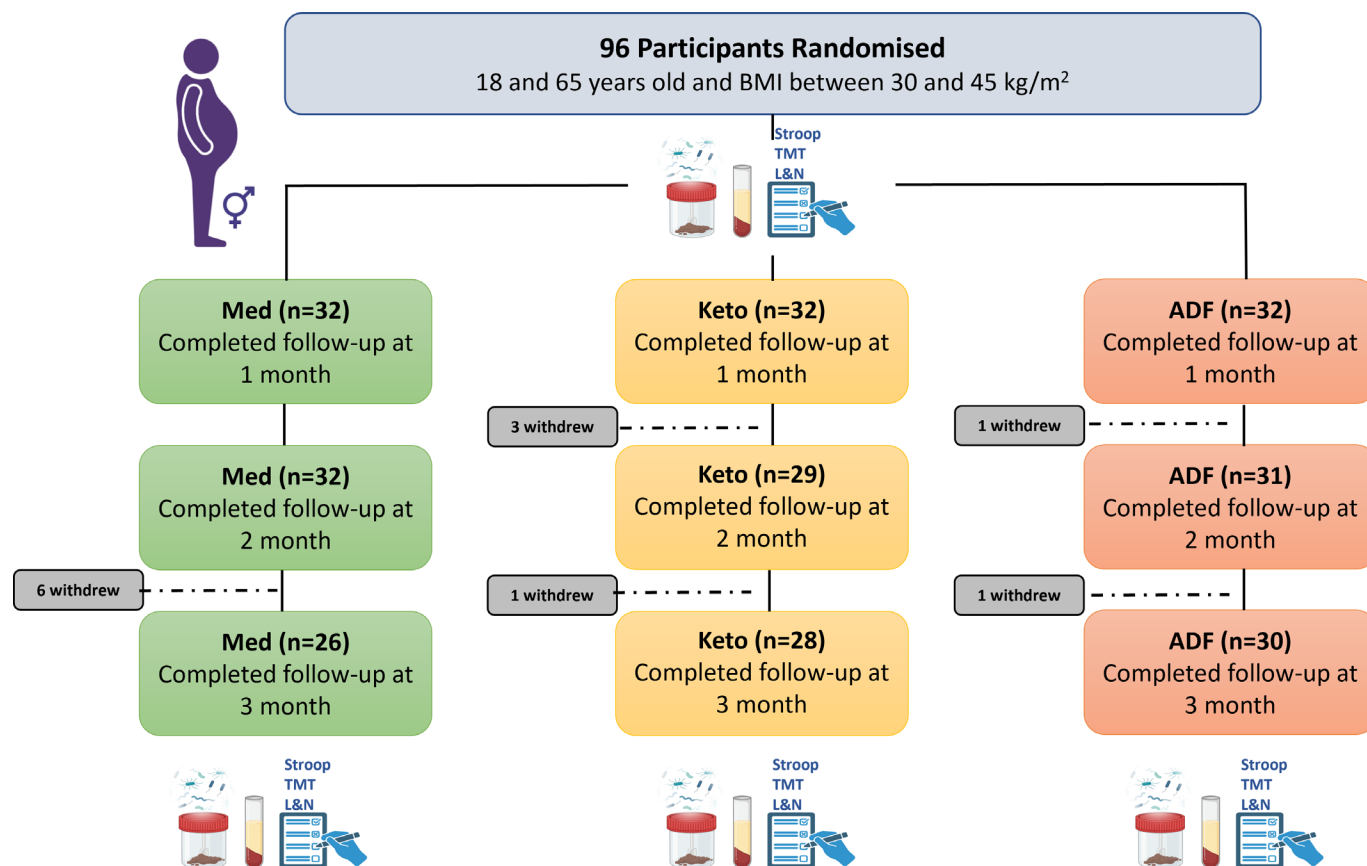


Figure 1 Participant flow diagram. Ninety-six healthy participants with obesity (32 per group, aged 18–65 years, body mass index (BMI) 30–45 kg/m²) were randomised into 3 months diet intervention: Mediterranean (Med), Ketogenic (Keto) and alternate-day fasting (ADF). Blood tests, faecal sample collection and cognitive assessments were performed. L&N, letter and number; TMT, trail making test.

of water and no-calorie beverages (eg, tea or coffee) was allowed during the fasting periods. The ADF intervention was isocaloric with respect to the other diets. Compliance with the different interventions was not specifically evaluated, although ketonaemia levels were assessed during the trial in all the study groups.

3. Keto diet was provided with a caloric deficit of 600 kcal/day and the following caloric distribution: 5% carbohydrates, 65% fats and 30% proteins of high biological value.

All participants received dietary counselling by expert nutritionists and written support materials and menus with the specific dietary plan to adhere to during the intervention (including detailed daily meals, specifying food portions) at baseline and follow-up sessions.

Human cognitive tests

Neuropsychological and psychometric tests were performed in every participant during the follow-up sessions: (1) Stroop test to measure the ease with which a person can shift his/her perceptual set to changing demands, and critically, to suppress a habitual response in favour of an unusual one. Different scores can be measured depending on the data used: word (W) for number of words accomplished in the first sheet, colour (C) for number of items accomplished in the second sheet, word-colour (WC) for number of items accomplished in the third sheet, $WP' = \frac{W \times C}{W + C}$ and Stroop interference resistance = $WC - WC'$; (2) letters and numbers from the Wechsler Adult Intelligence Scale (WAIS) span for working memory, concentration, auditory sequencing and executive attention; (3) trail making test (TMT) for visual

scanning/attention and working memory/task-switching analysis based on two steps: TMT A (rote memory) and TMT B (executive functioning). Only those participants with complete and available data were included in the current substudy. Improvement in cognitive performance was calculated by subtracting the score at baseline (prior to the diet intervention) from the score obtained at final condition (postdiet intervention). For statistical analysis, the body weight loss in kg was used as a covariable.

Human sample collection

Blood and stool samples were collected during the follow-up session from all the participants in overnight fasting condition (before breakfast).

Blood samples were collected for biochemical routine analysis as well as for serum and plasma isolation and stored in 0.25 mL aliquots. Peripheral blood mononuclear cells (PBMCs) were isolated for further analysis (see below).

Walnut-sized stool samples were collected in a sterile wide-mouth flask and promptly frozen at -80°C until further analysis.

Human faecal exosome isolation

Stool samples (300 mg) from individuals with obesity were used to isolate microbiota exosomes following manufacturer's instructions (ExoQuick, SBI, USA). After diluting 1:5 the faeces in Tris-EDTA buffer (Merck, Germany) and vortexing, the samples were filtered through a 40 μm nylon strainer and centrifuged at 4500g for 45 min at 4°C. The supernatant was incubated with phosphate-buffered saline (PBS)+0.5% polyvinylpyrrolidone

for 15 min with agitation. Afterwards, the sample was centrifuged at 13 000g for 3 min at 4°C and supernatant was incubated with ExoQuick precipitation solution overnight. Then, the sample was centrifuged at 1800 g for 35 min at 4°C and the pellet containing the exosomes was resuspended in PBS. Exosome concentration was measured using the Bradford assay (Bio-Rad, California, USA).

Metabolomics for exosome characterisation

The metabolomic analysis was conducted at oloBion, an omics bioscience laboratory. The sample preparation involved homogenisation with cold methanol using a grinder, followed by the addition of methyl tert-butyl ether containing an internal standard. The mixture was shaken and subsequently supplemented with 10% methanol. After an additional shaking step, the samples were centrifuged to separate the phases.

For metabolomic profiling, two aliquots of 70 µL of the bottom aqueous phase were collected and processed: (1) hydrophilic interaction liquid chromatography (HILIC) platform: the first aliquot was evaporated to dryness and resuspended in acetonitrile/water (containing an internal standard). The solution was shaken, centrifuged and analysed using HILIC; (2) reversed-phase liquid chromatography (RPLC) platform: the second aliquot was mixed with isopropanol/acetonitrile (1:1) mixture, shaken, centrifuged and the supernatant was evaporated and resuspended in 5% methanol containing internal standards. After shaking and centrifugation, the sample was analysed using RPLC. Chromatographic separation of polar metabolites was performed on Waters ACQUITY UPLC C18 BEH Amide and ACQUITY UPLC HSS T3 columns, both maintained at 45°C. The system was coupled to an Agilent 1290 Infinity UHPLC (Agilent Technologies) and a ZenoTOF 7600 system (SCIEX). The sample was injected in both electrospray ionisation positive and negative modes. For metabolite identification, the acquired data were processed and analysed using oloMAP V.2.0 (oloBion, Barcelona), an advanced data visualisation and interpretation platform for omics datasets.

Monocyte-derived microglia-like cells

PBMCs were isolated from participants' blood (both normo-weight individuals and participants with obesity, before and after the diet intervention) using a Ficoll gradient. PBMCs were cryopreserved in a fetal bovine serum (FBS)+10% dimethyl sulfoxide solution at -80°C. PBMCs were thawed in complete Roswell Park Memorial Institute (RPMI) medium (RPMI+10% FBS+1% penicillin/streptomycin) and seeded at 4×10^5 cells/cm². RPMI medium was changed every 3 days and supplemented with 100 ng/mL interleukin (IL)-34+10 ng/mL granulocyte-macrophage colony-stimulating factor.²⁵ After 14 days of differentiation, monocyte-derived microglia-like (MDMi) cells were used for further analysis (see below).

Monocyte-derived microglia-like cells treatment

MDMi cells derived from normo-weight volunteers were treated for 1 hour or 24 hours with RPMI+exosome (10 µg/mL) isolated from participants with obesity. The rationale behind these two time points was to evaluate distinct aspects of microglial response to microbiota-related stimuli. The short-term (1 hour) treatment was designed to assess the microglial cells' immediate and acute activation capacity, simulating an early phase response to microbial signals. In contrast, the long-term (24 hours) treatment aimed to investigate the effects of sustained exposure, reflecting a scenario in which prolonged stimulation may lead to

microglial overactivation, a state often associated with chronic inflammation and impaired functionality.

Microglial functional assays

Uptake of latex beads (fluorescent yellow-green; 1.0 µm particle size; Sigma-Aldrich, Ireland) was assessed in MDMi from normo-weight and donors with obesity prior and after the ADF intervention for phagocytic capacity analysis. MDMi differentiated from PBMCs (4×10^5 cells/well; 48 well-plate) were plated onto coverslips coated with matrigel (100 µg/mL; Corning, New York, USA). After 14 days in vitro, latex beads (0.025% in fresh RPMI media) were added to the wells, incubation continued for 4 hours, cells were washed, fixed in 4% paraformaldehyde and washed in PBT (PBS+1% Triton X-100) prior to staining. Cells were blocked (1 hour in PBT containing human serum albumin (3%)), incubated overnight (4°C) with primary antibody (rabbit anti-Iba-1; Wako, Japan; 1:1000), washed and incubated (2 hours; room temperature) with the secondary antibody (Alexa Fluor 546 donkey antirabbit IgG; 1:1000) and mounted in ProLong Gold with 4',6-diamidino-2-phenylindole (DAPI; Thermo Scientific, USA). Images (eight fields; 40× magnification) were acquired with a Leica SP8 Stellaris scanning confocal microscope (z-stack; four fields; 20× magnification) and processed using the ImageJ software (National Institute of Health, <https://imagej.nih.gov/ij/>; accessed 20 November 2021) and the number of latex beads⁺ cells was assessed.

To assess the motility of these cells, the wound healing assay based on drawing two scratches at right angles using a 10 µL pipette tip to create 'the wound' was used. Images were taken using a Nikon ECLIPSE TE2000-U microscope with a built-in camera (Nikon Metrology NV, Japan) at different intervals after the scratch and the width of the scratches was measured to quantify distance and speed travelled by the cells. In addition, a time-lapse was recorded as described below to add more specific data about their migration capabilities.

Microglial time-lapse studies

MDMi differentiated from PBMCs were seeded in an MW96 plate at a density of 2×10^5 cells/well in a final volume of 200 µL.

Treatment, fluorescent dyes and latex beads were added 1 hour prior to the assay. A time-lapse assay using the Operetta High Content Imaging System (PerkinElmer, Waltham, Massachusetts, USA), captured images every 20 min for 24 hours and 20 min under standard incubation conditions of temperature and CO₂. Image analysis used Harmony software V.4.8 (PerkinElmer).

Cell tracking was performed by assigning unique identifiers to individual cells to ensure accurate tracking throughout the experimental duration. Additionally, the fluorescent dye Sytox-Green was employed as a marker for cell death, facilitating the identification of viable cells until the conclusion of the observation period. Notably, the phagocytosis assay was exempt from the utilisation of SytoxGreen dye. It is worth noting that cells exhibiting movement out of the selected field of view or undergoing division were excluded from the analysis. In addition, the dye CellROX Deep Orange was used, and its measurement was always adjusted using the following formula in the segmentation of each cell:

Corrected intracellular ROS Signal :

$$\bar{X}_{CellROX_{ROS} INTRACELLULAR SIGNAL} = \bar{X}_{CellROX_{ROS} SIGNALING} - \bar{X}_{CellROX_{WHOLE CELL}}$$

Corrected ROS signal, eliminating the contribution from the surrounding region :

$$\bar{X}_{FI_{ROS} CORRECTED SIGNAL} = \frac{\bar{X}_{CellROX_{ROS} INTRACELLULAR SIGNAL}}{-\bar{X}_{CellROX_{SURROUNDING REGION}}}$$

The intensity measured outside the cell was obtained by selecting the surrounding region for each individual cell. Furthermore, each well was divided into six distinct fields of view for comprehensive data collection. Subsequently, the acquired images from the Operetta were subjected to analysis and processing employing the FIJI software (<https://imagej.net/contribute/citing>).

Multiplex/ELISA measurements

Serum from the participant before and after the dietary programme were used to analyse IL-10, IL-1 β , tumour necrosis factor- α (TNF- α), monocyte chemoattractant protein-1 (MCP-1), IL-6 and resistin by a multiplex assay (ProcartaPlex Human, Invitrogen). Samples and standards (25 μ L) were running in duplicate in a 96-well precoated plate (50 μ L capture beads mix) following manufacturer's instructions. After 2 hours incubation and several washes, the detection antibody mix (25 μ L) was added. After 30 min of incubation and several washes, streptavidin-PE mix (25 μ L) was added and incubated for another 30 min. Following a couple of washes, the plate was read using the xMAP system (Bio-Plex 200, Bio-Rad). For IL-10, IL-1 β and IL-6, most of the data were out of range.

Cell supernatant from MDMi samples was used to analyse IL-1 β , TNF- α and IL-6 by DuoSet ELISA Development Systems (R&D Systems, UK) as per the manufacturer's instructions. Absorbance was read at 450 nm using a BioTek Synergy HT microplate reader.

Animal studies

Male C57BL/6 mice (aged 8 weeks) were used in these experiments. Animals were housed (five per cage) under controlled conditions (20°C–22°C, food and water ad libitum) and maintained under veterinary supervision. Body weight and food intake were monitored weekly throughout the experiments. No adverse events were observed. Randomisation was employed to allocate mice to experimental groups in order to minimise bias.

Diet-induced obesity mice model and ketone bodies supplementation

A total number of 20 mice were fed with 60% of high fat diet (Brogaarden) for 6 weeks to induce an obesity phenotype. Afterwards, the chow diet was used to study the isolated effect of ketone bodies supplementation. A BHB supplement (KetoForce food supplement) was used at a concentration of 0.08 g/mL (final concentration of 4.2% BHB salt) in the drinking water of half of the animals (KB group), while the other half received plain drinking water and served as the control (Con) group. BHB concentration was based on previous literature outcomes demonstrating its effective range for modulating metabolic and immune responses, particularly within the 1–5 mM physiological range achieved during fasting or ketogenic states. This dosage has been shown to promote mitochondrial function, attenuate inflammation through NLRP3 inflammasome inhibition and act as a signalling metabolite via Histone Deacetylase (HDAC) inhibition and G Protein-Coupled Receptor (GPCR) activation.^{26 27} Fresh BHB suspension was prepared daily to avoid compound precipitation and maintain stability.

Faecal transplant mice model

A total number of 20 mice were depleted of their gut microbiota using an antibiotic suspension (ampicillin; 1 g/L) administered in their drinking water for 2 weeks prior to the faecal transplant procedure. Faecal transplants from human samples were

administered to the recipient animals by oral gavage over three consecutive days, following a 3-day washout period after antibiotic treatment. Each animal received a sample from a different donor (1:1 ratio). To maintain the microbiota transplant, a faecal boost was administered twice per week. One week before the start of the experiment, animals were handled by the experimenter and given drinking water via oral gavage to familiarise them with the procedure.

Novel object recognition test

The two-object variant of the novel object recognition (NOR) task was chosen to assay non-spatial memory in both animal models. The task consisted of three different stages: (1) habituation, (2) acquisition (training) and (3) testing. The habituation consisted of two sessions (2 days prior to the task; one session/day), where animals were placed for 10 min into the empty arena (cage-by-cage the first session or individually the second session). 24 hours after the second habituation session, two different objects constructed from standard Lego blocks were placed in the arena and mice were allowed to freely explore the two objects for 5 min. The criteria for exploration were based on active examination of the object by the animal, with the mouse touching the objects with at least its nose. The time spent exploring each object was recorded during the trial and animals were returned to their home cage when they completed the task. Animals that did not explore each object for at least 10 s were removed from the behavioural analysis. Twenty-four hours following acquisition, one familiar object was replaced with a novel object, and object exploration time was recorded over a 5 min period.

Mice sample collection

At the end of the experiment period, mice were anaesthetised with sodium pentobarbital (Euthanimal) and transcardially perfused with saline. Blood samples were collected by cardiac puncture prior to perfusion. The brains were dissected and used for immunohistochemical analysis and gene expression studies (see below).

Immunohistochemistry

The brain was dissected and fixed in 4% paraformaldehyde for 24 hours for immunohistochemical analysis. Following fixation, the tissue was incubated in 30% sucrose for 48 hours for cryoprotection and then frozen in isopentane. Tissue was embedded in optimal cutting temperature solution, and 20 μ m coronal sections were prepared using a cryostat. Sections were stored at –20°C in a freezing solution (30% ethylene glycol, 30% sucrose in PBS) until required for immunohistochemistry.

The immunohistochemical study was performed on brain slices containing the medial hippocampus. Sections were washed and permeabilised in PBT, blocked (1 hour in PBT containing bovine serum albumin (3%)), incubated overnight (4°C) with primary antibody (anti-PFKFB3 (1:250; AB96699, Abcam, UK); anti-Iba1 (1:1000; 019-19741 WAKO or 1:700; AB5076, Abcam, UK); anti-p16 (1:200; AB54210, Abcam, UK); anti-CD68 (1:350; AB303565, Abcam, UK); anti-Ki67 (1:250; AB279653, Abcam, UK); anti-Syn (1:250; sc-17750, Santa Cruz); anti-GLUT5 (1:250; sc-271055, Santa Cruz)), washed and incubated (2 hours; room temperature) with the secondary antibody (Alexa Fluor 546 (1:1000, A11010, Invitrogen); Alexa Fluor 568 (1:1000, A21124, Invitrogen); Alexa Fluor 488 (1:1000, A48286, Invitrogen) and Alexa Fluor 647 (1:1000, A32849TR, Invitrogen)). Prior to mounting the tissue, DAPI staining (1:8000; D1306,

ThermoFisher) was used for nuclei visualisation (10 min at RT). Brain tissue was mounted in ProLongGlass Antifade Mountant (P36984, ThermoScientific). Images were captured using a Leica SP8 Stellaris scanning confocal microscope (three fields; 40× magnification) and processed using the ImageJ software.

Microglia cell morphology and three-dimensional reconstruction

Image stacks (0.5 µm step size; 33 steps) were taken from Iba1-stained hippocampal tissue sections (20 µm) using a Leica SP8 Stellaris scanning confocal microscope, and image stacks were converted to three-dimensional (3D) images. Microglia 3D reconstruction and analysis were conducted using the ImageJ 3D Suite plugin. Initially, z-stacks containing microglia cells were imported in their original format. Subsequently, adjustments to brightness and contrast were made to optimise visualisation. Cells displaying clear nuclei and branching structures were then selected for analysis, using rectangle selection tools and subsequently duplicated for further processing. Employing the 3D OC options settings, parameters of interest were selected. A critical step involved selecting an appropriate threshold using the 3D object counter to ensure minimal background interference while capturing the full microglia structure within the image. Threshold selection was determined based on the overall quality of the micrograph and the intensity of background noise. The image adjustment threshold command was then employed, with the minimum value set to 1 and the maximum value set to 3. In the 3D manager settings, parameters of interest such as Volume, Fill Ellipse, Surface, Feret, Bounding Box, Compactness and Centroid were chosen. Then, the images were added to the 3D viewer command for visual evaluation. This step involved examining the fabricated image to ensure that the generated morphology accurately represented the primary images. Special attention was given to verifying the absence of structures in the background that might be erroneously identified as part of other cells. If multiple objects appear to represent the same cell within the image, they were merged. After acquiring one image per cell, the Measure 3D command was used to extract relevant parameters characterising the morphology and features of the microglia cells from each image. Subsequently, the extracted data were exported to Excel for further interpretation.

Further analysis of microglia morphology was performed using the FracLac ImageJ plugin. Images were converted to 8-bit greyscale, a threshold was set and binarised images were filtered by pixel size to reduce background and enhance contrast. Soma diameter, cell perimeter and area were assessed, and the process number and length, as well as the number of junctions and triple and quadruple points/cell, were quantified.

Gene expression

RNA, isolated from mouse hippocampus and MDM human samples using a Nucleospin RNAII kit (Macherey-Nagel, Germany), was reverse transcribed into complementary DNA (cDNA) using a high-capacity cDNA Archive kit according to the manufacturer's instructions (Applied Biosystems, UK), and real-time PCR was performed using Kapa probe fast (VWR, KK4702) on duplicate samples with predesigned Taqman gene expression assay for IL-6 (Mm00446190_m1), IL-1β (Hs01555410_m1), TREM2 (Hs00219132_m1), CD68 (Hs02836816_g1), GLUT5 (Hs01086390_m1), PFKFB3 (Hs00998698_m1), APOE (Hs00171168_m1), TNF-α (Hs00174128_m1) using a CFX 96 Real Time System. Samples were assayed with β-actin

(VIC/MGB probe, primer limited, 4352341E for mouse tissue and 4326315E for human cells, ThermoFisher) as the endogenous control to normalise gene expression data. Gene expression was calculated relative to the endogenous control genes and normalised to the control sample, yielding relative quantification values using the $2^{-\Delta\Delta CT}$ method, where CT represents the threshold cycle.

Protein expression

Protein samples isolated from mouse hippocampus tissue using the column flow-through of the Nucleospin RNAII kit (Macherey-Nagel) were incubated in lysis buffer (Tris-HCl 1 M, thiourea 2 M, urea 70 mM, 4% 3-[(3-Cholamidopropyl) dimethylammonio]-1-propanesulfonate (CHAPS); Sigma, UK), equalised for protein concentration, and then mixed with 4× sodium dodecyl sulfate (SDS) sample buffer (composition: Tris-HCl 100 mM, pH 6.8, 4% SDS, 2% bromophenol blue, 20% glycerol; Sigma, UK). The samples were then boiled at 95 °C for 5 min. Samples were applied to 10%–15% SDS gels, proteins were transferred to polyvinylidene difluoride membrane, non-specific binding was blocked (5% non-fat dried milk powder in Tris-buffered saline containing 0.05% Tween 20) and membranes were incubated overnight at 4°C with rabbit anti-IL1β antibody (1:750 in blocking buffer; 500-P51-100UG, PeproTech) or mouse anti-actin (1:5000 in blocking buffer; A5316, Sigma, UK). Membranes were washed and incubated (room temperature, 2 hours) with a secondary horseradish peroxidase-linked antirabbit (1:2000 in blocking buffer; 111-035-003, Jackson, USA) or antimouse (1:10 000 in blocking buffer; 115-035-003, Jackson, USA) antibody. Bands were detected using WesternBright ECL chemiluminescent substrate (Bio-Rad, USA) and images (ChemiDoc Imaging System, Bio-Rad, USA) were evaluated using ImageJ (<http://rsb.info.nih.gov/>).

Microbiota analysis

DNA extraction from stools was done using the QIAamp DNA stool Mini kit (Qiagen). Gut microbiota was assessed through the 16S rRNA sequencing with the 16S Metagenomics Kit (Thermo Fisher Scientific). Libraries were created using the Ion Plus Fragment Library Kit (Thermo Fisher Scientific). Barcodes were added to each sample using the Ion Xpress Barcode Adapters kit (Thermo Fisher Scientific). Emulsion PCR and sequencing of the amplicon libraries were performed on an Ion 530 chip (Ion 530TM Chip Kit) using the Ion Torrent S5TM system and the Ion 510/520/530TM Kit-Chef (Thermo Fisher Scientific) according to the manufacturer's instructions. The process included reference *Escherichia coli* samples for quality assessment. After sequencing, the individual sequence reads were filtered using Ion Reporter Software V.4.0 to remove low-quality and polyclonal sequences and further translated into amplicon sequence variants using DADA2 with adapted parameters for Ion Torrent data within the microbiome analysis package QIIME2 (www.qiime2.org),²⁸ which will also be used for diversity analysis and subsequent taxonomic analysis through Analysis of Composition of Microbiomes with Bias Correction (ANCOM-bc). The PICRust plugin was also used within QIIME2 in order to infer the metabolic metabolism of the microbiota population.

Metabolite quantification by ^1H NMR spectroscopy

All spectra were acquired on a Bruker AVANCE 600 MHz Spectrometer (Bruker BioSpin, Ettlingen, Germany) equipped with an *Advance III* console and either a 4 mm TXI ^1H high-resolution magic angle spinning (HR-MAS) probe for intact tissue analysis or a nitrogen-cooled TCI Prodigy cryoprobe for plasma samples analysis.

Water-suppressed HR-MAS NMR spectra of intact tissue samples were acquired using a Carr-Purcell-Meiboom-Gill (CPMG) sequence with the following parameters: 12 kHz spectral width, 64 000 data points, 64 scans, 1 ms echo time (2τ) with a total echo time of 130 and 5 s relaxation delay. Water presaturation was applied during the relaxation delay. Metabolite quantification was performed using the LCModel software,²⁹ as described elsewhere,³⁰ with creatine as the internal reference.

For plasma samples, the following acquisition sequences were used: one-dimensional (1D) Nuclear Overhauser Effect Spectroscopy, 1D CPMG for T_2 editing of macromolecule signals and 2D J-resolved (JRES) to aid in the identification of metabolites. Small metabolites were quantified from the CPMG spectra using Chenomx software (V.10.0, Chenomx, Edmonton, Canada), with the Electronic Reference To Access In Vivo Concentrations (ERETIC), as implemented in TopSpin 3.5.pl7 (ERETIC 2), serving as the concentration reference.

Statistical analysis

All statistical analyses were performed using SPSS V.28.0.1.1, GraphPad Prism 9 and QIIME2. The Kolmogorov-Smirnov and Levene tests were used to assess normality and homoscedasticity, respectively. Data are reported as the mean (\pm SEM), with the number of experimental individuals or repetitions indicated in each figure. For human studies, only datasets with both basal and final parameters were included. For animal studies, only mice that learnt the task during the behavioural test were included. Statistical analysis was carried out using Student's t-test for two independent means or analysis of variance followed by Tukey's post hoc test, as appropriate. A Spearman's correlation test was performed when required. The significance level was set at $p < 0.05$.

RESULTS

Diet-induced ketonaemia triggers greater body weight loss, cognitive improvement and changes in gut microbiota

Table 1 shows anthropometric and biochemistry blood measurements at the basal and final stages of the diet intervention. BMI, waist and hip circumference were decreased with the three diet interventions, with the most significant outcomes in the Keto group ($p < 0.05$). Fat, lean and muscle mass (kg) were also decreased with all diets, but again, the most significant results were found in the Keto group ($p < 0.05$; $p < 0.01$; $p < 0.001$, respectively). Vitamin D was increased after the diet intervention in every group with the highest concentration in the Keto group ($p < 0.05$). Ketonaemia can only be measured at the final stage since levels are under the detectable limits at basal levels. Ketonaemia increased in the three groups, showing higher levels in the Keto ($p < 0.01$) and ADF ($p < 0.01$) group compared with the Med group.

Significant changes were observed in body weight (figure 2A) and BMI (figure 2B) (final-basal measurements), with a similar decrease in the Keto and ADF groups compared with the Med group ($p < 0.05$). Although the decrease in fat mass tended to

be more prominent in the Keto and ADF groups, there were no significant differences between groups (figure 2C). However, the basal metabolism rate was higher after 3-month ADF intervention compared with the Keto group (figure 2D; $p < 0.01$).

Regarding cognitive performance, the inhibitory control measured by the Stroop test was better after the ADF intervention (figure 2E; $p < 0.05$). However, the working memory measured by the letter and number (L&N) test (figure 2F) was equally improved by Keto and ADF interventions ($p < 0.05$). TMT A and B outcomes explore the visual attention of the participants, where the Keto group showed worse improvement in TMT A compared with the Med and ADF groups (figure 2G; $p < 0.05$). Combining these outcomes, ADF intervention was more successful in cognitive improvement than the other dietary interventions.

In order to investigate gut microbiota diet-related changes, 16S rRNA analysis was performed in the faeces of the individuals before and after diet intervention. Although no differences were found in alpha and beta diversity (online supplemental figure S1A-C), particular changes in the abundance of bacteria population distribution were associated with each dietary programme (figure 2H). Nine depleted and nine enriched bacteria genera were found after the 3-month dietary interventions. On the one hand, the depleted genera populations were: (1) after ADF intervention: *Romboutsia*, *TM7x*, *Eubacterium_hallii_group*, *Granulicatella* and *Dorea*; (2) after Keto intervention: *Klebsiella*, *Paraclostridium*, *Muribaculaceae* and *Incertae_Sedis*. On the one hand, the enriched genera populations were: (1) after ADF intervention: *Leuconostoc*, uncultured genus from *Oscillospirales* order, *DTU014* and *Victivallis*; (2) after Keto intervention: *Actinomyces*, *Aeromonas* and (3) after Med intervention: *Akkermansia*, *Pseudoflavonifractor*, *Eubacterium_ruminantium_group*. Additionally, a Spearman's correlation test was performed to analyse the relationship between the microbiota bacteria population and the cognitive performance of the individuals after the different dietary programmes (figure 2I). Interestingly, a strong positive correlation was found between the *Agathobacter* genus and TMTB ($p < 0.01$). *Bilophila* and *Actinomyces* were positively correlated with Stroop interference scores ($p < 0.05$), and *Bilophila* also showed a positive correlation with the TMT A performance ($p < 0.05$). *Dorea* was negatively correlated with the TMT B scores ($p < 0.05$). *DTU014* genus was positively correlated with L&N test ($p < 0.05$). To understand the inferred metabolic pathways, we performed the Phylogenetic Investigation of Communities by Reconstruction of Unobserved States (PICRUSt) analysis (online supplemental figure S1D). This analysis revealed that the Med diet only affected one pathway (PWY-3801), which was enriched after the diet intervention. In comparison, the Keto diet affected 19 pathways (14 depleted and five enriched routes), most of which were related to aromatic compound degradation, while ADF affected only four pathways (three enriched and one depleted). Interestingly, PWY-3081 (amino acid biosynthesis) and Lactosecat-PWY (carbohydrate degradation) were enriched in the ADF and Keto groups, respectively, along with PWY-6948 (fatty acid and lipid degradation).

Fasting pattern intervention decreased the inflammatory state of people with obesity

Since the participant's cognitive performance could not be explained by the increase in ketone bodies due to the lack of differences between groups, we decided to explore the anti-inflammatory effects of the different diet interventions. We found a significant decrease in the ADF group of ferritin (figure 3A)

Table 1 Clinical and metabolic parameters for participants who complete the study before and after 3 months with Med, Keto or ADF diets

	BASAL			3 Months		
	Med	Keto	ADF	Med	Keto	ADF
Sex (W/M)	18/8	23/5	16/14	18/8	23/5	16/14
Age (years)	47.92±9.68	45.14±11.28	46.93±8.20	47.92±9.68	45.14±11.28	46.93±8.20
BMI (kg/m ²)	38.15±4.98	36.86±5.25	40.07±6.26	35.03±4.73	32.06±4.44†	35.35±5.25
Waist (cm)	116.15±12.71	112.67±12.28	122.49±15.1	104.41±12.01	101.43±13.2†	111.3±14.28
Hip (cm)	127.61±9.90	124.6±12.26	128.5±12.38	120.72±10.51	116.07±11.8†	120.83±13.09
Glucose (mg/dL)	95.12±12.96	92.72±9.70	99.97±17.51	94.52±12.95	91.28±9.26	95.38±12.96
Trig (mg/dL)	125.68±80.11	116.33±49.57	150.94±71.8	111.19±37.75	98.24±40.03	114.58±42.18
Chol (mg/dL)	187.44±34.03	196.82±28.46	194.88±45.03	189.65±35.53	196.17±33.78	189.54±49.62
HDL (mg/dL)	48.42±10.90	50.31±11.47	44.21±10.39	48.32±9.4	49.34±13.57	47.58±12.74
LDL (mg/mL)	114.84±28.98	123.77±24.44	120.44±37.48	119.06±28.78	127.14±13.57	119±41.37
Apoa1 (mg/day)	145.65±54.25	158.89±22.54	144.12±33.02	161.76±31.36	156.2±30.73	154.71±28.47
Apob (mg/dL)	98.38±20.71	100.94±20.50	105.24±27.67	99.2±27.35	102.46±20.44	99.43±26.71
AST (U/L)	25.75±8.09	25.47±14.10	27.71±8.30	21.18±5.34	27.47±20.39	18.82±4.79
ALT (U/L)	33.12±17.14	31.63±22.94	30.27±15.08	23.74±10.82	32.59±28.06	23.63±7.77
Fat mass (%)	41.05±5.32	41.44±5.52	38.61±5.63	38.48±4.74	36.90±7.08	34.95±7.92
Fat (kg)	43.80±10.30	42.48±11.26	49.7±15.99	38.05±8.60	32.35±9.55†	36.72±11.48
Lean (kg)	60.58±13.60	57.62±10.80	67.77±15.88	60.09±13.23	54.48±10‡	66.46±14.58
Muscle (kg)	59.0875±12.6	55.98±9.23	68.65±11.61	57.28±12.51	51.76±9.5§	64.48±12.25*
TBMR (kcal/day)	1908.17±402	1807.88±309	2216.59±395	1839±408.15	1652.6±290§	2057.5±385*
VitD (mg/dL)	27.88±7.46	23.81±6.36	23.29±7.13	33.54±12.11	31.17±14.48†	28.16±12.57*
Urea (mg/dL)	34.61±7.19	35.47±9.44	38.18±8.62	36.29±9.39	37.62±10.02	36.67±9.0
Ketonaemia (mM)	–	–	–	0.16±0.15	0.53±0.32¶	0.35±0.32*
3-Hydroxybutyrate (µM)	46.62±58.59	110.64±273.90	60.78±70.42	81.54±27.73	184.23±280.88	133.87±332.01
Acetate (µM)	27.80±9.13	28.30±8.14	53.71±123.90	45.02±45.05	41.18±29.40	62.74±164.13
Acetoacetate (µM)	21.50±22.08	41.14±76.46	30.25±31.41	35.40±30.28	58.95±75.30	45.52±84.05
Acetone (µM)	16.56±11.41	32.25±53.27	25.04±23.41	34.71±44.25	58.59±72.42	44.79±75.12

Data are means±SD.

Analysis of variance and Tukey's multiple comparison test between all the groups.

*P<0.05 vs Med.

†P<0.05 vs ADF.

‡P<0.01 vs ADF.

§P<0.001 vs ADF.

¶P<0.01 vs Med.

ADF, alternate-day fasting; ALT, alanine aminotransferase; Apoa1, apolipoprotein a1; Apob, apolipoprotein b; AST, aspartate aminotransferase; BASAL, before diet intervention and 3 months after intervention; BMI, body mass index; CF, cardiac frequency; Chol, cholesterol; HDL, high-density cholesterol; IndCal, indirect calorimetry; Keto, ketogenic diet; LDL, low-density cholesterol; Med, Mediterranean diet; TBMR, theoretical basal metabolic rate; Trig, triglycerides; VitD, vitamin D; W/M, woman/men.

and MCP-1 (figure 3C) compared with Keto (p<0.01) and Med (p<0.05), respectively. Although the decrease in resistin concentration did not reach significant values between groups, it was more prominent in the ADF group than the rest (figure 3B), suggesting that the ADF pattern provides anti-inflammatory effects. To further investigate the anti-inflammatory effects of the ADF pattern, MDMi cells from participants were studied in vitro before and after ADF intervention to analyse their functionality. Microglial phagocytic capacity (figure 3D-E,I) and oxidative stress (figure 3F) were increased in MDMi after diet intervention (p<0.001; p<0.005, respectively). Additionally, those cells showed higher displacement and speed than prior to diet intervention (figure 3G and 3H; p<0.05), and this was associated with a better wound healing capacity (figure 3J; p<0.05), suggesting that ADF overall improved microglial function.

Microbiota obesity-related changes negatively affect human monocyte-derived microglia-like cells

To investigate whether microglial function could mediate the correlation between microbiota changes and cognitive performance in obesity, MDMi cells derived from normal-weight

participants were pretreated for 1 hour or treated for 24 hours with faecal exosomes isolated from the participants before the diet intervention (figure 4). The 1-hour treatment condition increased the phagocytic capacity of those cells (figure 4A-B; p<0.001); however, under 24-hour treatment, these cells exhibited impaired phagocytic activity (figure 4F-G; p<0.001), suggesting that in the short term, microglial cells become activated by the treatment, whereas prolonged exposure leads to overactivation and a subsequent loss of phagocytic function. Analysing the oxidative stress of those cells, we found an increase with the pretreatment (figure 4C; p<0.001), corroborating the activation of the cell due to the 1-hour treatment. No differences were found in displacement or speed during the pretreatment (figure 4D,E). However, the 24-hour treatment decreased the wound healing capacity of these cells (figure 4H; p<0.05).

A massive increase in IL release (TNF-α; IL6 and IL-1β) was found in the supernatant of the treated cells (figure 4I-K; p<0.01; p<0.05 and p<0.05, respectively). These results confirmed the inflammatory state of these cells after being stimulated for 24 hours with obesity-related exosomes. To further explore the microglial state, RT-qPCR tested a batch of different

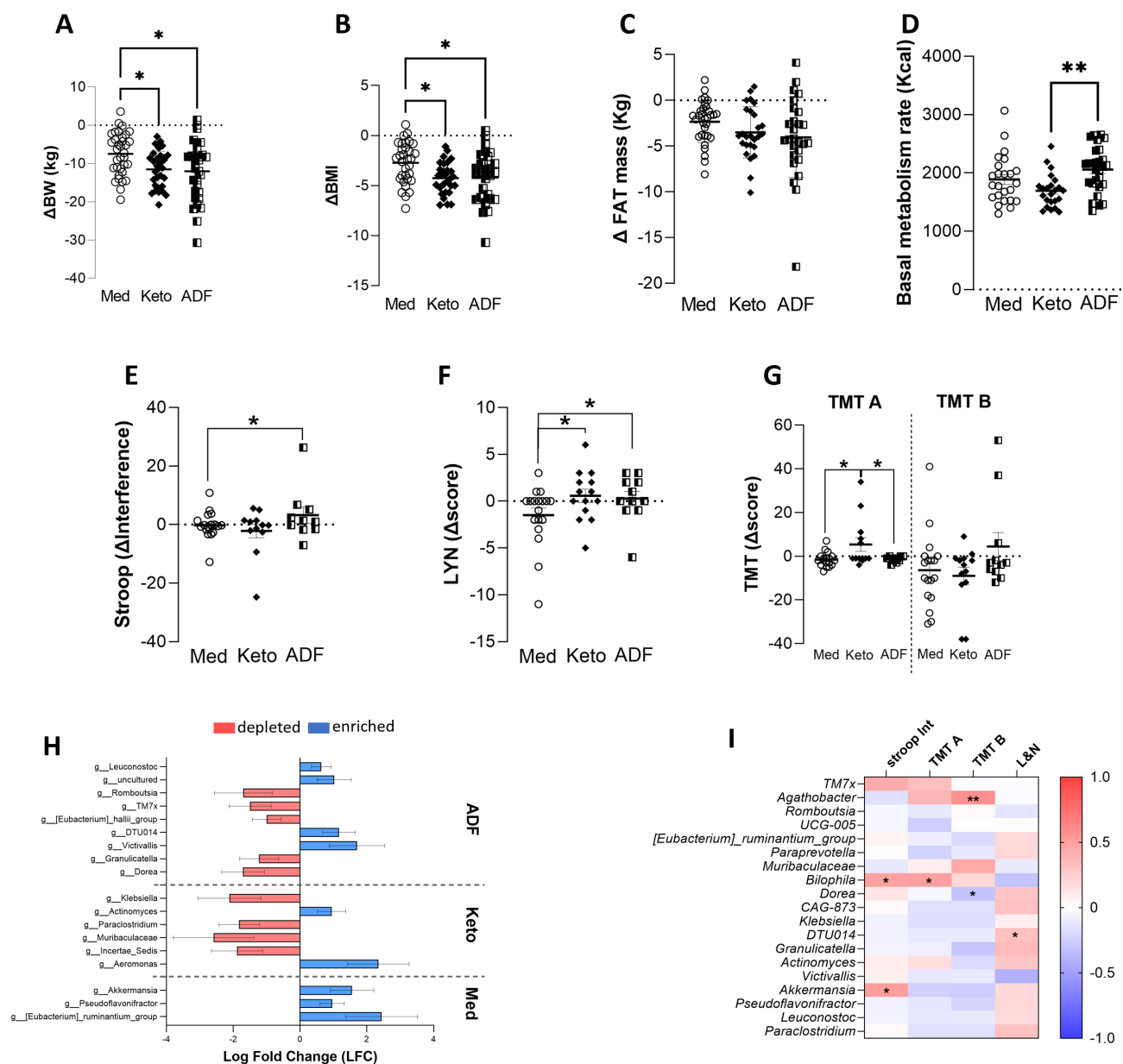


Figure 2 Diet intervention based on ketone body increase reduced body weight in people with obesity and improved their cognitive performance associated with microbiota changes. (A) Body weight changes (Δ BW) in kilograms (kg) were higher in the ketogenic (Keto) and alternate-day fasting (ADF) groups compared with the Mediterranean diet (Med). (B) Body mass index changes (Δ BMI) were higher in Keto and ADF groups compared with Med. (C) No changes were found in fat mass changes (kg) between groups. (D) Basal metabolism rate (kcal) was increased in ADF compared with Keto group. (E) Better improvement in the Stroop cognitive test (Δ interference) was found in ADF compared with Med group. (F) Better improvement in the letter and number (L&N) test (Δ score) was found in Keto and ADF compared with Med group. (G) Worse improvement in the trail making test A (TMT A) score (Δ score) was observed in the Keto group compared with the ADF and Med groups. No changes were found in task B of this cognitive test. (H) Significant changes in enriched and depleted bacteria genus due to diet intervention in the individuals who underwent the cognitive test evaluations (n=11–17). (I) Heatmap represents positive (red) or negative (blue) correlation between microbiota diet-related changes and cognitive scores. One-way analysis of variance was used for the A–D dataset (n=23–34). Cognitive performance was analysed by one-way analysis of covariance using body weight loss as a covariable in E–G (n=10–17). ANCOM-bc analysis was used for H data representing log fold change \pm SE. Spearman's correlation test was run for heatmap representation in I. * $P < 0.05$, ** $p < 0.01$.

genes for MDMi phenotyping (figure 4L). TREM2 messenger RNA (mRNA) expression was downregulated with the 24 hours exosome treatment compared with the control group, corroborating their low phagocytic capacity ($p < 0.01$). Although there were no significant changes in the rest of the analysed genes, a tendency to increase overactivation markers (IL-1 β , PFKFB3, CD68 and TNF- α) was found among the results.

Ketone body supplement affects body weight, cognitive performance and hippocampal inflammation in a DIO mice model

To discard the implication of increased ketone bodies in the beneficial effects of ADF pattern on cognitive performance and inflammatory state, we investigated the effects of ketone bodies

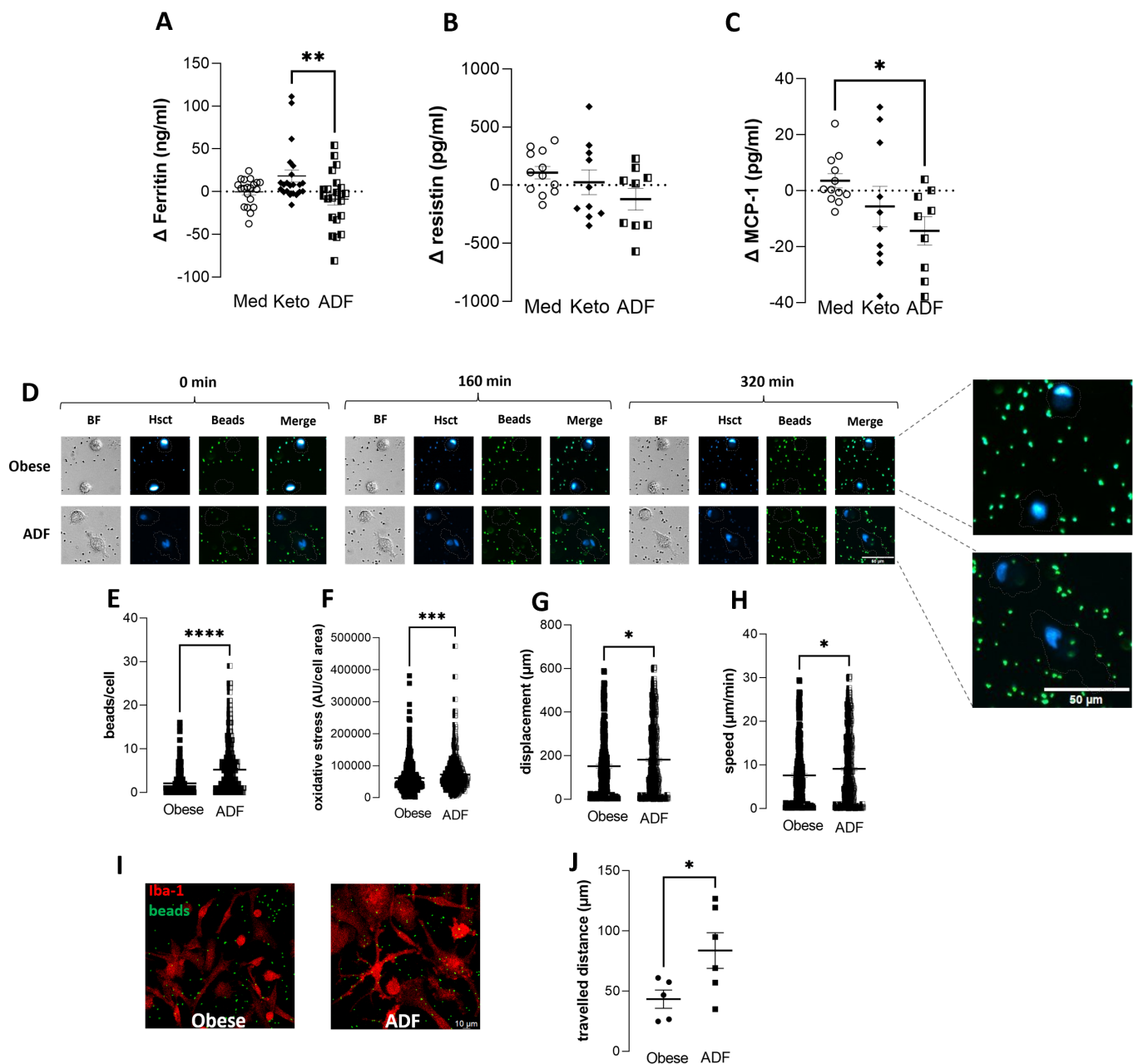


Figure 3 Alternate-day fasting (ADF) intervention improved systemic inflammation in people with obesity and promoted better functionality in human monocyte-derived microglia-like (MDMi) cells. Different inflammatory markers linked to obesity were analysed in serum samples from participants under the different diet interventions (Med: Mediterranean diet; Keto: ketogenic diet; ADF). In addition, human MDMi cells isolated from the participant's blood before (obese group) and after (ADF group) diet intervention were cultivated to corroborate the inflammatory state of the individuals. (A) Ferritin increment (Δ) in ng/mL after diet intervention was significantly lower in ADF compared with Keto group. (B) No significant changes were found in Δ resistin (pg/mL), although ADF showed a trend towards a decrease after the intervention. (C) A significant decrease in Δ monocyte chemoattractant protein-1 (MCP-1; pg/mL) was found in the ADF group compared with Med group. (D) Representative micrographs of MDMi timelapse studies for latex beads engulfment as a measure of phagocytic capacity prior to and after ADF intervention. (E) The greatest number of beads/cells was engulfed by the ADF group. (F) Higher levels of oxidative stress were shown by ADF group. (G, H) Increased motility capacity (displacement and speed) was found in the ADF group. (I) Representative micrographs of Iba-1 (microglial marker) and latex beads staining from MDMi participant cells before and after ADF. (J) Functional improvement by ADF intervention in MDMi travelled distance during the wound healing assay. Data are expressed as the mean (\pm SEM). One-way analysis of variance was used for the A–C dataset (n=9–22). The Student's t-test was performed in the cellular study (E–H: n=60–200 cells from 3/6 different participants for single cell analysis; J: n=5 participants). *P<0.05, **p<0.01, ***p<0.005, ****p<0.001.

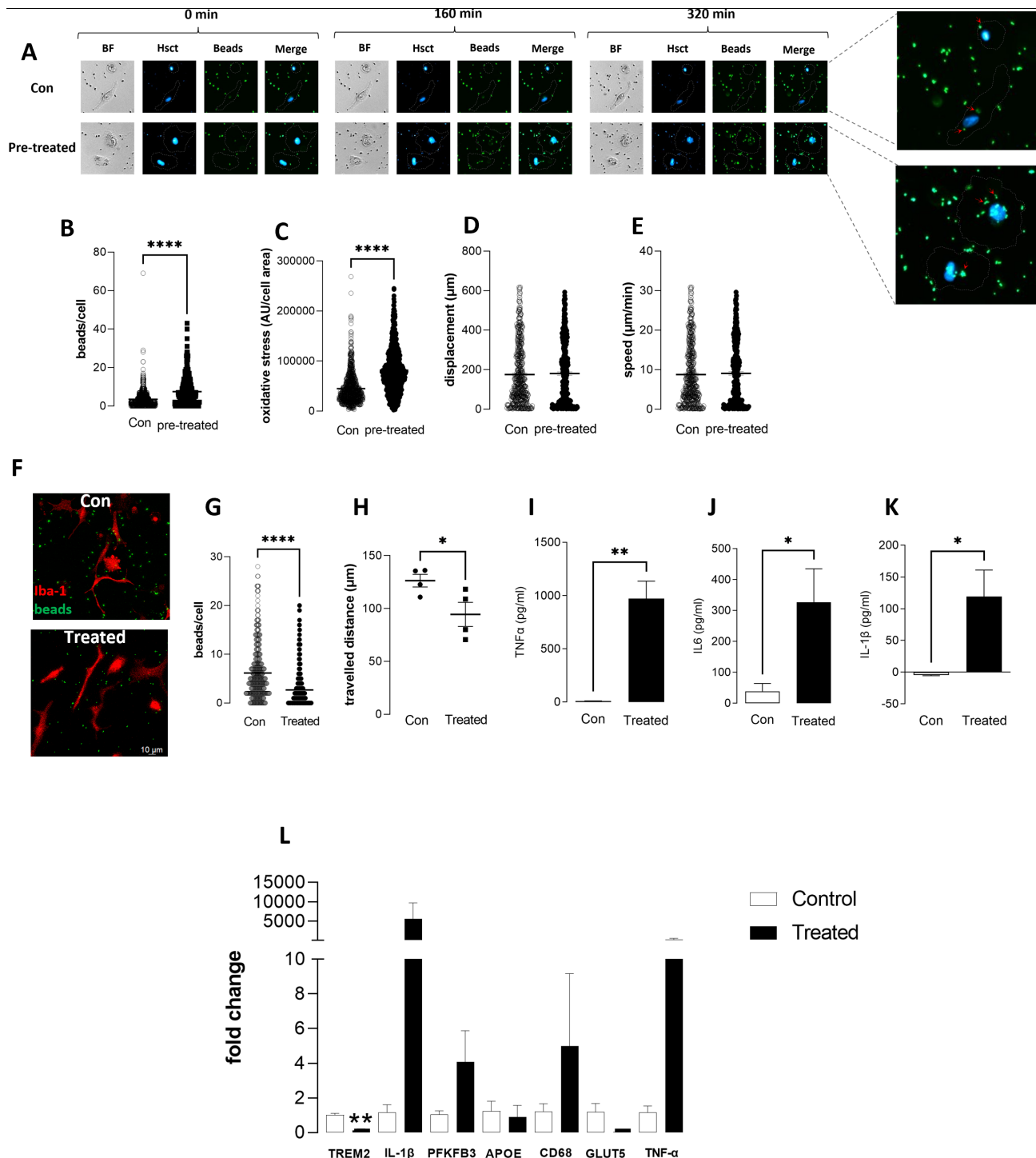


Figure 4 Human monocyte-derived microglia-like (MDMi) cells increase their phagocytic capacity in response to acute microbiota-related changes associated with obesity, while they exhibit functional collapse under chronic stimulation. Human MDMi cells, isolated from the healthy donors' blood were pretreated (1 hour) or treated (24 hours) with microbiota-derived exosomes (10 μg/mL) from participants before the dietary intervention to characterise microglial activation and function. (A) Representative micrographs of MDMi timelapse studies for latex beads engulfment as a measure of phagocytic capacity under short-term (1 hour) microbiota obesity-exosome pretreatment. (B) The greatest number of beads/cells was engulfed by the pretreated group. (C) Higher levels of oxidative stress were shown by the pretreated group. (D, E) No differences were found regarding motility capacity. (F) Representative micrographs of Iba-1 (microglial marker) and latex beads staining from the two experimental groups (control vs treated: 24 hours treatment). (G, H) Functional impairment (beads engulfment and travelled distance during the wound healing assay, respectively) in MDMi cells due to chronic exposure (24 hours) to the exosome treatment. (I–K) Increase in cytokines (tumour necrosis factor alpha (TNF-α); interleukin 6 (IL-6); interleukin 1 beta (IL-1β)) release from MDMi cells after the exosome 24 hours treatment. (L) Battery of different genes related to microglial activation and phenotype. Only a significant decrease was found in TREM2 expression due to the chronic exposure (24 hours) to microbiota exosomes. Data are expressed as the mean (±SEM). The Student's t-test was performed for statistical analysis (n=60–200 cells from 3/6 different participants for single cell analysis, n=3–6 for the rest of analysis). *P<0.05, **p<0.01, ****p<0.001.

alone in a diet-induced obesity (DIO) mouse model, aiming to isolate their impact from other intermediate effects associated with dietary intervention. Although the ketone body supplementation significantly reduced the body weight of DIO mice during the experiment (online supplemental figure S2A; $p < 0.001$), no significant changes were observed in cognitive performance (online supplemental figure S2B) or hippocampal microglial activation as a result of the supplementation (online supplemental figure S2C–D). To confirm the effectiveness of the supplement, different ketone bodies were analysed in the blood of these animals. A significant increase in 3-hydroxyisobutyrate (online supplemental figure S2E; $p < 0.05$) and acetate (online supplemental figure S2H, $p < 0.05$) was observed, along with a trend towards increased 3-hydroxybutyrate (online supplemental figure S2F; $p = 0.052$) in the supplemented group. However, 1,3-dihydroxyacetone was significantly decreased by the supplement (online supplemental figure S2G; $p < 0.005$), although its primary substrate, acetone, appeared to increase in response to the ketone body supplement (online supplemental figure S2I).

The gut microbiota profile of these animals was analysed to identify taxa resembling those observed in the human study (online supplemental figure S2JJ). Although alpha diversity did not differ between groups, the overall gut microbiota composition was significantly different (PERMANOVA; $p < 0.001$). ANCOM-bc analysis at the genus level showed six enriched genera—*Akkermansia*, *Lachnospiraceae_UCG-006*, *Parabacteroides*, *Rikenellaceae_RC9_gut_group* and two uncultured genera from the order Rhodospirillales and the Peptococcaceae family—as well as nine depleted genera, including *Butyrivibrio*, *Roseburia*, *Lactobacillus*, *Muribaculaceae*, *Eubacterium_coprostanoligenes*, *Tuzzerella*, *Mucispirillum* and one uncultured genus from the Lachnospiraceae family. Notably, several bacterial genera modulated by the supplement in animals were also identified in the human intervention study. For instance, *Akkermansia*, which was enriched in the supplemented animals, was similarly increased in participants following the Mediterranean diet. Similarly, *Muribaculaceae*, which was significantly depleted in animals, showed a parallel depletion in the Keto group in humans. These shared taxa suggest a degree of cross-species response to dietary interventions, reinforcing the translational relevance of the findings.

Human microbiota diet-related changes modify cognitive performance linked to neuroinflammation in healthy mice

After 6 weeks of faecal transplant, the ADF-recipient mice improved their cognitive performance in the short-term and long-term, compared with the obese-recipient mice (figure 5A,B; $p < 0.001$). cFos and Arc mRNA expression (figure 5C,D) were measured due to their impact on NOR performance. ADF-recipient mice showed higher levels of both markers than the obese-recipient mice ($p < 0.05$).

Regarding hippocampal inflammation, we found a decrease in IL-6 mRNA (figure 5E; $p < 0.05$) and IL-1 β protein levels (figure 5F–G; $p < 0.01$) in ADF-recipient mice compared with obese-recipient mice. This neuroinflammation reduction was also associated with decreased microglial numbers and densitometry (figure 5H–I; $p < 0.01$; $p < 0.05$, respectively), suggesting that obese-recipient microglia are overactivated. To confirm this fact, we expand the microglial analysis to study its morphology. Figure 5K represents the different parameters studied for microglial morphology, where ADF-recipient mice showed huge differences from obese-recipient mice in all the parameters analysed. ADF-recipient mice showed bigger

perimeter/cell (online supplemental figure S3E; $p < 0.001$); radius from centre (online supplemental figure S3E,F; $p < 0.001$); a more significant number of junctions, slab and end points per cell (online supplemental figure S3G–I; $p < 0.001$), lower volume and surface area (online supplemental figure S3L,N; $p < 0.001$ and $p < 0.05$, respectively) than microglia from the obese-recipient mice. Microglial cells from the ADF-recipient group showed smaller soma and a greater number of branches (figure 5L–M; $p < 0.001$) than microglia from obese-recipient mice. No changes were observed in the remaining morphological parameters analysed (online supplemental figure S3A–D,J–K,M).

Human microbiota diet-related changes affect microglial phenotype in healthy mice

To better understand the implication of microglial cells in GMBA communication, we analysed functionality and proliferation/senescence markers in the hippocampal region of those animals that received the human faecal transplant.

PFKFB3 expression in microglial cells was evaluated as another marker of microglial overactivation since it has been shown that microglial cells, when overactivated, switch into a more glycolytic phenotype, as previously described by the authors.^{31–33} Figure 6A,B showed a decrease in ADF-recipient mice of Glut5_PFKFB3_Iba-1⁺ cells compared with obese-recipient mice ($p < 0.001$).

To analyse phagocytic capacity in those cells, the colocalisation of CD68 with synaptophysin signal was measured in Iba-1⁺ cells (figure 6C,D). In this case, obese-recipient mice showed a loss of function in their phagocytic capacity compared with the ADF-recipient group ($p < 0.005$).

Whether those events were related to microglial senescence processes or cell turnover was also investigated by analysing p16 and Ki67 in Iba-1⁺ cells. Obese-recipient mice showed higher numbers of senescent microglial (p16_Iba-1⁺ cells) than the ADF-recipient group (figure 6E,F; $p < 0.05$). Regarding microglia cell turnover, ADF-recipient mice showed higher numbers of Ki67_Iba-1⁺ cells than the obese-recipient group (figure 6G,H; $p < 0.001$).

Human microglia cell-type is affected by microbiota diet-related changes

To decipher whether diet intervention changes microbiota metabolite composition and to find a biomarker to help us understand the microglial modifications found in our animal model, exosomes from human microbiota were isolated for further analysis by metabolomic profiling.

Figure 7A showed a volcano plot with the most significant metabolites found in the microbiota exosome of participants with obesity who underwent ADF dietary intervention.

An increase in riboflavin ($p < 0.01$) and citrulline ($p < 0.05$), two metabolites linked to brain energy and neuroprotection, was found after the diet intervention (figure 7B). Neurotransmitter precursors, such as tryptophan, glutamine-alanine and glycine-leucine, were increased after the diet intervention (figure 7C; $p < 0.05$). Structural and synaptic support metabolites, such as threonine-threonine and isoleucine-serine, were increased after the diet intervention (figure 7D; $p < 0.05$). N-epsilon-acetyllysine and thymidine, metabolites related to DNA and epigenetic regulation, were also increased after the diet (figure 7E; $p < 0.05$). Online supplemental figure S6 shows the rest of the significantly differentiated metabolites due to the diet intervention.

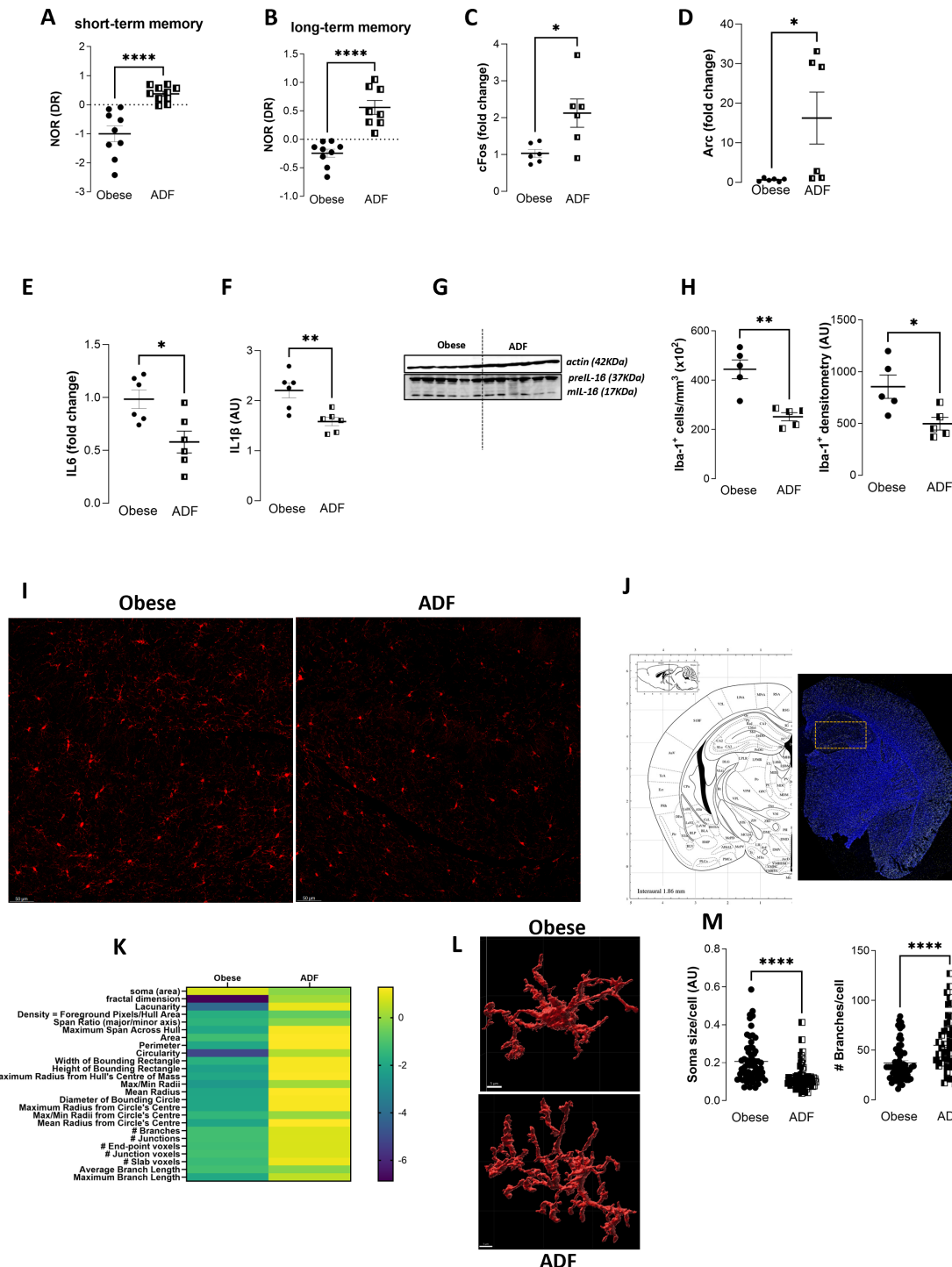


Figure 5 Microbiota changes associated with alternate-day fasting (ADF) ameliorate obesity-related cognitive decline by modulating hippocampal inflammation, neuronal activation and microglial morphology in healthy recipient mice. To directly assess the impact of these microbiota alterations on cognitive function and hippocampal physiology, faecal transplants were performed in healthy C57BL/6J mice using samples from human participants collected before (obese) and after the ADF intervention. (A, B) The novel object recognition (NOT) discrimination ratio (DR) was increased in ADF-recipient mice at short-term and long-term time points. (C, D) Higher hippocampal neuronal activation was shown by ADF-recipient mice. (E, F) Higher levels of interleukin-6 (IL-6) and interleukin-1 beta (IL-1β) were shown by obese-recipient mice. (G) Immunoblots from pre-IL-1β, mature IL-1β and actin measurement. (H) Iba-1⁺ (microglial marker) cells and their densitometry showed an increase in the obese-recipient mice. (I) Representative micrographs of Iba-1 staining from the two experimental groups. (J) Mouse brain atlas (left) and representative micrographs showing DAPI staining. The analysed region in all immunohistochemistry assays—the dentate gyrus (DG)—is highlighted in orange. (K) Heatmap showing the different morphological parameters analysed in this study (Z-score). ADF-recipient mice differ completely from the obese-recipient group in terms of microglial morphology. (L) Representative three-dimensional microglial reconstruction from the two experimental groups. Data are expressed as the mean (±SEM). (M) Morphological parameters (soma size and number of branches per cell) in microglia from the two experimental groups. Obese-recipient mice showed larger soma size than ADF-recipient mice, while ADF-recipient mice showed a greater number of branches. The Student's t-test was performed for statistical analysis (n=5–10). *P<0.05, **p<0.01, ****p<0.001.

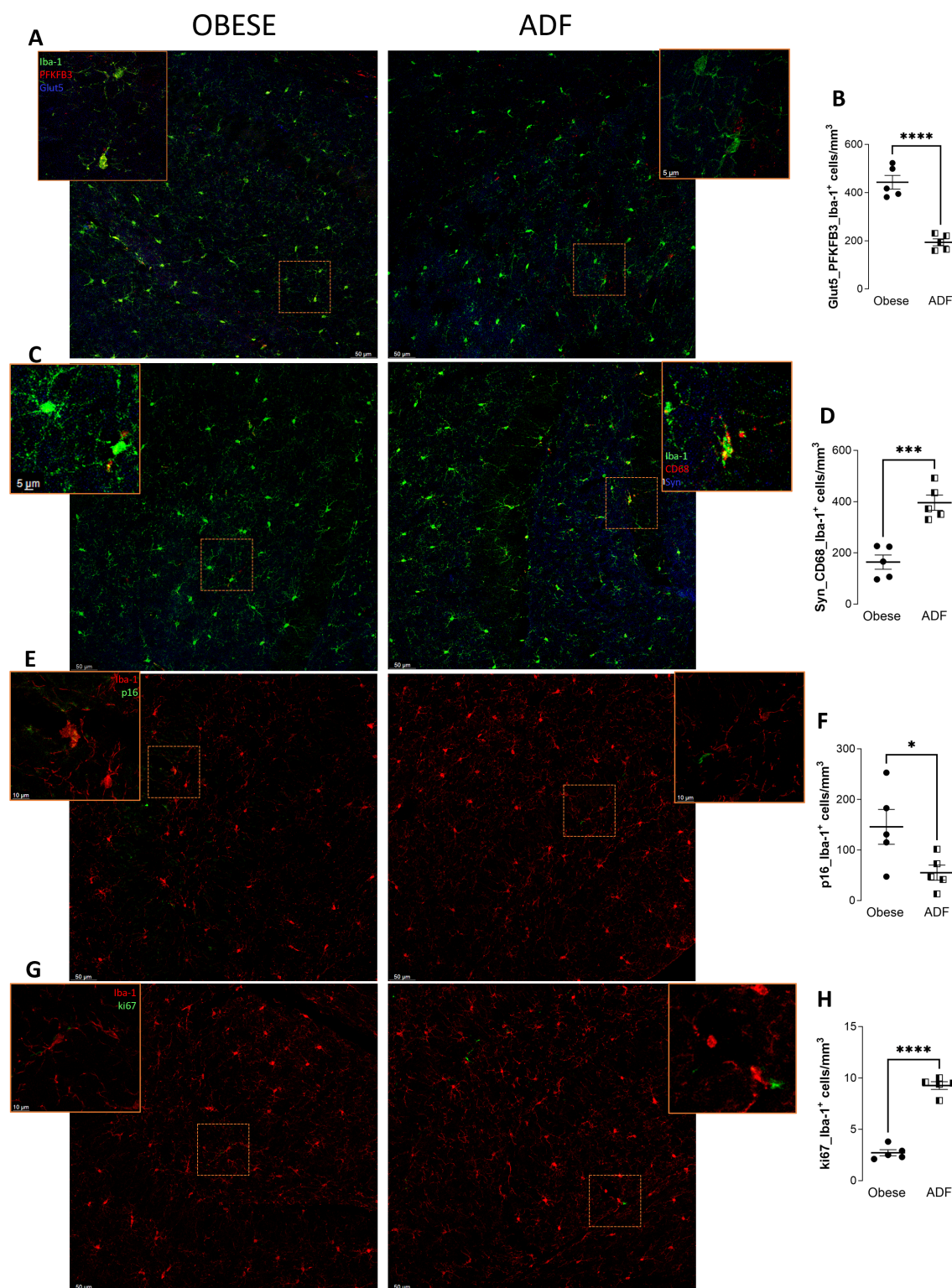


Figure 6 Microglial overactivation due to microbiota obesity-related changes is associated with loss of function and microglial senescence. A faecal transplant from the human participant before (obese) and after alternate-day fasting intervention (ADF) was performed in healthy recipient mice (C57BL/6J) to better understand the direct effect of microbiota changes in microglial activation, function and state. (A) Representative micrographs of Iba-1 (microglial marker), Glut5 (glucose receptor 5), PFKFB3 (glycolytic enzyme) staining from the two experimental groups. (B) The greatest number of Glut5_PFKFB3_Iba-1⁺ cells were found in the obese-recipient mice, indicating a glycolytic state of microglial cells. (C) Representative micrographs of Iba-1, CD68 (lysosomal marker) and synaptophysin (Syn; presynaptic molecule) staining from the two experimental groups. (D) The greatest number of phagocytic microglia (Syn_CD68_Iba-1⁺ cells) were found in ADF-recipient mice. (E) Representative micrographs of Iba-1 and p16 (senescence marker) staining from the two experimental groups. (F) Higher number of senescent microglia (p16_Iba-1⁺ cells) were found in obese-recipient mice. (G) Representative micrographs of Iba-1 and ki67 (cell turnover marker) staining from the two experimental groups. (H) Higher number of ki67_Iba-1⁺ cells were found in ADF-recipient mice. Data are expressed as the mean (±SEM). The Student's t-test was performed for statistical analysis (n=5). *P<0.05, ***p<0.005, ****p<0.001.

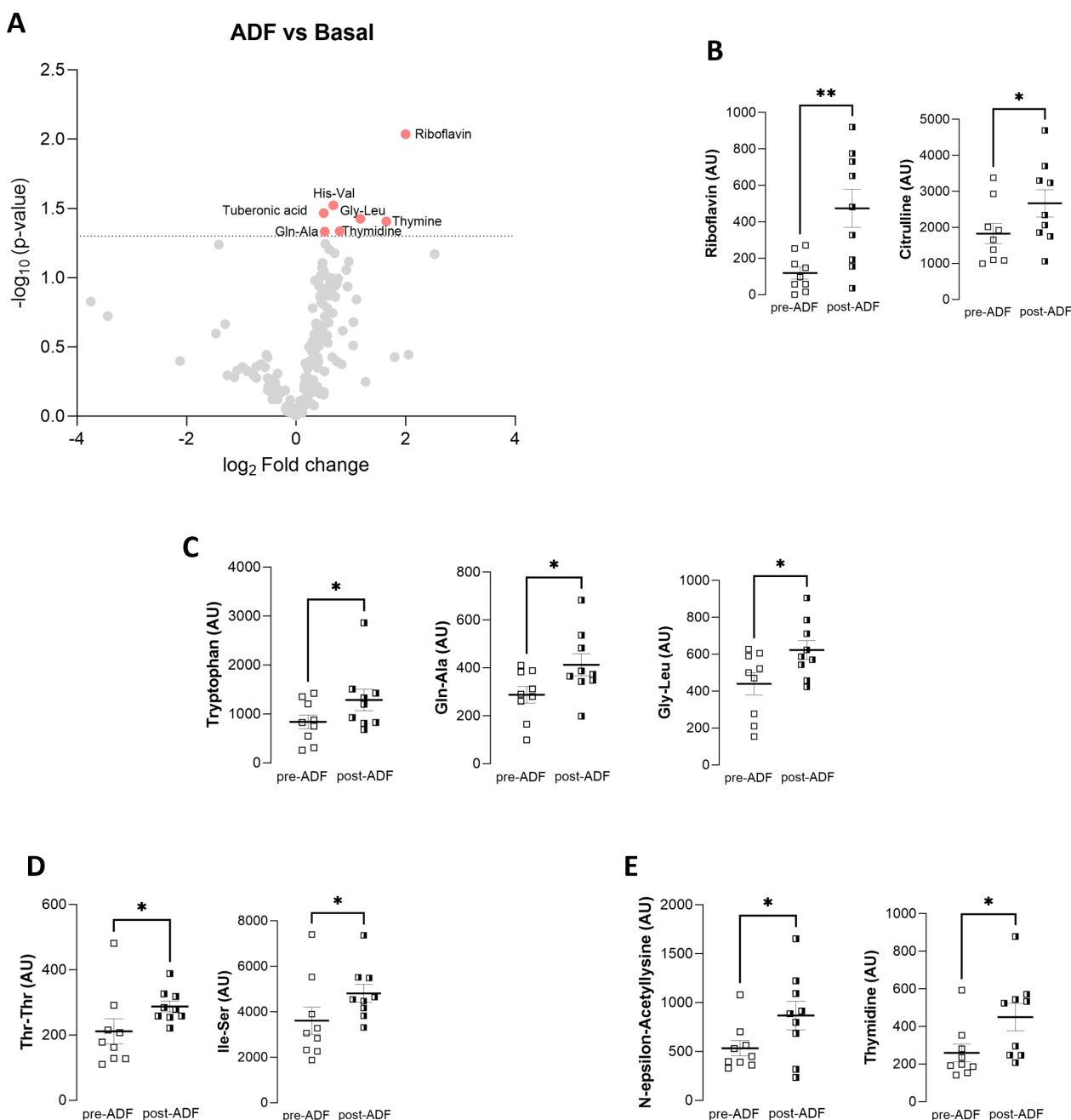


Figure 7 Metabolomic microbiota changes in response to the alternate-day fasting (ADF) intervention. Exosomes were isolated from the participants' faecal samples before and after ADF intervention to analyse changes in different metabolites due to the diet. (A) Volcano plot showing the most significant differentiated metabolites due to the ADF intervention. (B) Upregulation of riboflavin and citrulline due to ADF intervention. (C) Upregulation of tryptophan, glutamine-alanine (Gln-Ala) and glycine-leucine (Gly-Leu) due to ADF intervention. (D) Threonine-threonine (Thr-Thr) and isoleucine-serine (Ile-Ser) were upregulated due to the ADF intervention. (E) N-epsilon-acetyllysine and thymidine were upregulated due to the ADF intervention. Data are expressed as the mean (\pm SEM). The Student's t-test (paired) was performed for statistical analysis (n=9). * $P < 0.05$, ** $p < 0.01$.

DISCUSSION

In this study, we demonstrated that a weight-loss dietary programme could ameliorate the obesity-related cognitive decline reported in the literature and that different patterns result in different outcomes. Our initial hypothesis focused on the role of ketone bodies, given their capacity to modulate energy metabolism and neurotransmitter activity,^{34–36} particularly BHB, which increases during both ketogenic diets and fasting. Indeed, prior studies have shown BHB's influence on cognitive performance, as confirmed by a recent Mendelian

randomisation analysis linking elevated BHB levels to improved cognition.³⁷ While we observed the highest BHB levels in participants following the ketogenic diet, it was the ADF group that showed the greatest cognitive improvement, suggesting that ketone body levels alone do not fully explain the cognitive benefits. This led us to explore the source and context of ketone body production, as these influence their systemic effects. Endogenous BHB produced during fasting is increasingly recognised for its anti-inflammatory and signalling functions, such as NLRP3 inflammasome suppression, a key microglial intracellular sensor,

mechanisms that differ from exogenous or dietary BHB.^{38–40} This fact was reinforced in our DIO mouse model, where exogenous BHB supplementation, although effective in reducing body weight, had limited effect on cognition and did not modulate hippocampal microglia, underlining the importance of the metabolic context.⁴¹ To further understand the mechanisms beyond the ketone bodies surge after the different diet interventions, we examined systemic inflammation, particularly its impact on microglial cells, the brain's resident immune cells. Among all the interventions, ADF had the strongest anti-inflammatory effect, both systemically and at the cellular level. Microglial cell type from the ADF group showed enhanced phagocytic function and a less inflammatory profile. These findings support the idea that microglial modulation is a key link in the GMBA, mediating cognitive outcomes associated with dietary interventions. It has been shown that microglial cells play a crucial role in cognition by regulating synaptic pruning, neuroinflammation and neuronal connectivity; their balanced activity supports learning and memory, while chronic activation or dysfunction contributes to cognitive decline observed in ageing and neurodegenerative diseases.^{42–45} This immune modulation is closely tied to gut microbiota composition, which shifts significantly in obesity and contributes to chronic low-grade inflammation.⁴⁶ Our MDMi model using cells from healthy donors but treated with microbiota-derived exosomes from participants with obesity demonstrated how gut-derived signals impair microglial function, especially under prolonged stimulation, which mimicked chronic exposure in obesity. Interestingly, we found that the human microglial cell type shows higher phagocytic capacity under acute stimulation than the non-stimulated cells. However, after chronic stimulation, they completely lost their function, and this was associated with lower levels of TREM2, a marker of dysfunctional microglia implicated in neurodegenerative processes.^{47–50} This dataset suggests that microbiota diet-related changes affect microglial function and could mediate the long-term cognitive decline induced by the neuroinflammation associated with obesity.

Moving from descriptive to mechanistic insights, we explored whether the diet-induced microbiota changes themselves could be responsible for the observed effects since different studies have shown changes in microbiota composition due to diet-induced ketosis.^{51–56} Indeed, several taxa were differentially regulated in both human and mouse models, suggesting a shared microbial signature underlying cognitive improvements. Interestingly, the *Dorea* genus, linked to cognitive impairment,^{57,58} was depleted following the ADF diet and negatively correlated with TMT B, supporting the cognitive performance improvement after ADF intervention. DTU014, which was enriched in the ADF group, was linked to cognitive improvement by its positive correlation with L&N score, supporting the beneficial effect on cognitive performance of this diet intervention. *Akkermansia*, whose beneficial effects on cognition have been previously reported,⁵⁹ was significantly enriched in the Med group and positively correlated with Stroop interference scores, corroborating its benefits in cognitive performance. This overlap between species supports the idea that specific microbial taxa may act as therapeutic targets.

Since diet-related changes did not fully align with increases in ketone bodies and cognitive test scores, we decided to investigate these effects separately. Supplementation with BHB in the DIO mice model confirmed the known benefits of ketone bodies in promoting body weight loss. However, only a slight improvement in cognitive performance was observed, suggesting that factors other than BHB alone may be responsible for the

cognitive benefits observed with the dietary intervention. Interestingly, BHB-supplemented animals shared the outcomes of *Akkermansia* and *Muribaculaceae* abundance with the Med and Keto diet, two genera associated with cognitive performance, especially the depletion of *Muribaculaceae* has been linked to better performance in the NOR and open field test.^{60,61} Since BHB supplementation did not result in shared bacterial genera with ADF diet intervention, the lack of cognitive improvement in the DIO mouse model may be attributed to the absence of ADF-specific microbiota changes, rather than the increase in ketone bodies alone.

Given the strong communication between the gut microbiota and brain function via the GMBA,⁶² we sought to explore how diet-related changes in human microbiota could affect cognitive function in healthy recipient mice. We replicated previous data from other research groups demonstrating that obesity-related changes in the microbiota can impair cognitive function in healthy animal.^{24,62} Furthermore, we showed that ADF-related microbiota changes improve cognitive performance in both the short and long term, and these changes were associated with reduced hippocampal inflammation mediated by microglial cells. It seems plausible that a healthier microglial phenotype (larger spread cell, ramified and smaller soma) shows higher phagocytic capacity and cell turnover, as we found in the ADF-recipient mice. In addition, due to microbiota obesity-related changes, glycolytic microglial cells increased senescent markers, which could be related to the observed hippocampal inflammation and loss of memory in the obese-recipient mice.

Throughout this study, we provide strong evidence that diet-induced microbiota changes can influence cognitive performance in healthy animals, highlighting microglial cells as key mediators in this process. However, further experiments are needed to connect all the pieces of this puzzle and show a real connection between these events and uncover the underlying molecular mechanisms. Considering that GMBA communication relies on vagal stimulation through the enteric nervous system⁶³ and gut microbiota metabolites that can travel through the circulation to the brain,⁶⁴ we extended our molecular studies to characterise microbiota-derived metabolites in the human donors before and after the ADF intervention. Interestingly, all significantly altered metabolites were upregulated following the ADF intervention, and many have been previously associated with cognitive improvement through enhanced brain energy and neuroprotection. Among these, riboflavin (vitamin B₂) was notably elevated. Riboflavin is known to inhibit the production of pro-inflammatory cytokines (eg, TNF- α , IL-6, IL-1 β) by modulating nuclear factor kappa B (NF- κ B) and NLRP3 signalling pathways, thereby playing a key role in mitigating obesity-related inflammation and supporting mitochondrial function.^{65,66} In fact, riboflavin has recently been recognised for its role in modulating microglial activation and reducing neuroinflammation. In particular, its metabolism via riboflavin kinase—an enzyme highly expressed in microglia during inflammatory states—has been shown to regulate immune signalling through NF- κ B pathway. Prior work in AD mouse models have demonstrated that microglial-targeted riboflavin derivatives reduce amyloid- β burden and restore cognitive function,⁶⁷ further supporting riboflavin as a plausible mediator of the cognitive benefits observed in our study.

Our studies show the importance of dietary intervention in cognition regardless of body weight loss or the highest ketosis induction, as other research groups suggested in the past. In fact, when we analysed the sole effect of high concentrations of ketone bodies in animals with obesity, we

only observed improvement in body weight loss without significant effects on cognitive performance, suggesting the presence of another key player. Moving to faecal transplant models, we found how different microbiota changes affect cognitive performance in healthy mice. Notably, ADF-related microbiota changes led to the most significant modifications in microglial cells, further corroborating our findings from human and cellular studies. Surprisingly, when we characterised the metabolites released by human microbiota after the ADF intervention, we identified riboflavin as a key mediator of the diet's beneficial effects on microglial function and cognitive, corroborating previous outcomes from other researchers. Together, these findings reinforce the notion that dietary interventions influence cognition through metabolic regulation and via gut microbiota-driven modulation of immune pathways, particularly through microglia. The ADF intervention appears to be the most effective strategy, triggering a favourable shift in the microbiota, reducing inflammation, improving microglial health and enhancing cognition. While the BHB and ketone bodies contribute supportively, our data suggest that metabolites such as riboflavin and specific microbial taxa (eg, *Akkermansia*) may serve as more potent mediators of these beneficial effects.

Overall, our findings shed light on the mechanisms underlying GMBA communication, highlighting the importance of microglial health as a key mediator in preventing obesity-associated cognitive decline. Nevertheless, further studies are required to determine whether microglial cells are essential components of GMBA signalling.

Limitations of the study

Our study presents some limitations to consider. Although this study is part of a randomised clinical trial, the sample size for the human studies was limited by the fact that individuals are exposed to several factors that could hinder regimen adherence or success. Additionally, to avoid bias from the day of the week or time of cognition assessment, a fixed schedule was established for data collection, which made the task unsuitable for everyone. Regarding the animal models, although antibiotic-treated mice are a validated model for faecal microbiota transplantation, they are not fully germ-free, which could potentially affect some outcomes. However, to validate the effectiveness of our approach, we assessed microbial depletion in the antibiotic-treated animals and confirmed that over 80% of bacterial genera were successfully eliminated. While not entirely germ-free, this level of microbial depletion provides a robust and practical model for evaluating microbiota-driven effects. Finally, our use of 16S rRNA amplicon sequencing limits taxonomic resolution to the genus level, thereby restricting the depth of microbial identification and functional inference. Despite this limitation, 16S rRNA sequencing remains a widely accepted, robust and cost-effective method for gut microbiota profiling, supported by well-curated and standardised reference databases. While more advanced techniques such as whole-genome shotgun metagenomics offer higher taxonomic and functional resolution, they are still evolving in terms of accessibility, standardisation and cost-effectiveness.

Author affiliations

¹Department of Endocrinology and Nutrition, Instituto de Investigación Biomédica de Málaga y Plataforma en Nanomedicina-IBIMA Plataforma Bionand, Málaga, Spain

²Center for Biomedical Network Research in Physiopathology of Obesity and Nutrition (CIBEROBN), Instituto de Salud Carlos III, Madrid, Spain

³Department of Endocrinology and Nutrition, Hospital Universitario Virgen de la Victoria-IBIMA Plataforma Bionand, Málaga, Spain

⁴Department of Biological Models, Vilnius University, Vilnius, Lithuania

⁵Biomedical Magnetic Resonance Laboratory-BMRL, Fundación Pública Andaluza Progreso y Salud (FPS), Seville, Spain

⁶Biomedical Magnetic Resonance Laboratory-BMRL, Instituto de Investigación Biomédica de Málaga y Plataforma en Nanomedicina-IBIMA Plataforma Bionand, Málaga, Spain

⁷Biomedical Research Networking Center in Bioengineering, Biomaterials & Nanomedicine (CIBER-BBN), Instituto de Salud Carlos III, Madrid, Spain

⁸Department of Molecular Biology and Biochemistry, Facultad de Ciencias, Universidad de Málaga, Málaga, Spain

⁹Molecular Basis of Biological systems (SIBIUMA), Instituto de Investigación Biomédica de Málaga y Plataforma en Nanomedicina-IBIMA Plataforma Bionand, Málaga, Spain

¹⁰Center for Biomedical Network Research in Rare Diseases (CIBERER), Instituto de Salud Carlos III, Madrid, Spain

¹¹Department of Medicine and Dermatology, Facultad de Medicina, Universidad de Málaga, Málaga, Spain

Correction notice This article has been corrected since it published Online First. Table 1 and the data availability statement have been updated.

X Virginia Mela @MelaNeurobio

Contributors Conceptualisation: IMI and FJT; methodology: VM; investigation: VM, VH, MI, MLG-M, MB and JDP-G; writing—original draft: VM; writing—review and editing: VM, IMI and FJT; funding acquisitions: IMI and FJT; resources: JIM-M, AMG-P and BB; supervision: VM; project administration: IMI and FJT. VM acted as guarantor.

Funding This work was supported by Principal Investigators' grants from the Instituto de Salud Carlos III (PI18/01160, PI21/01677, PI24/00347), as well as UMA-FEDERJA-116 and PY20-00447 from the Junta de Andalucía, and co-funded by FEDER funds, for which we are very grateful. VM, VH, AS-V and IMI contracts are supported by the Instituto de Salud Carlos III (CP22/00033, CD22/00144, FI22/00193, CPII21/00013). NMR spectra acquisition was carried out at the U28 Unit of the ICTS 'NANBIOSIS' at IBIMA Plataforma BIONAND. MB's contract is supported by the Ministerio de Ciencia e Innovación and the Universidad de Málaga (IJC2018-037657-I and A.4 Fellowship II Plan Propio, University of Málaga). JIM-M was supported by a Río Hortega grant from the Instituto de Salud Carlos III, Madrid, Spain (CM22/00217).

Competing interests None declared.

Patient and public involvement Patients and/or the public were not involved in the design, or conduct, or reporting, or dissemination plans of this research.

Patient consent for publication Not applicable.

Ethics approval This study was approved by the Ethics Research Committee of Malaga (PI18/01160) and conducted according to the principles of the Declaration of Helsinki. All participants provided written informed consent before enrolment in accordance with the provisions of Regulation (EU) 2016/679 General Data Protection and Organic Law 3/2018, of 5 December, of Protection of Personal Data and guarantee of digital rights and Law 14/2007, of 3 July, on Biomedical Research. All experiments and animal protocols were reviewed and approved by the local Ethics Committee and complied with Royal Decree 1201/2005 (BOE No. 252) on the protection of experimental animals, as well as with Directive 86/609/EEC of the Council of the European Communities. The experiments were conducted in accordance with the guidelines and protocols established in Royal Decree 53/2012 on the care and protection of animals used for scientific purposes.

Provenance and peer review Not commissioned; externally peer reviewed.

Data availability statement Data are available on reasonable request. Original data from NMR are available at Zenodo (doi.org/10.5281/zenodo.15333296); 16S rRNAseq data are deposited in the SRA under PRJNA1136827 and PRJNA1257837. All other data are available upon reasonable request.

Supplemental material This content has been supplied by the author(s). It has not been vetted by BMJ Publishing Group Limited (BMJ) and may not have been peer-reviewed. Any opinions or recommendations discussed are solely those of the author(s) and are not endorsed by BMJ. BMJ disclaims all liability and responsibility arising from any reliance placed on the content. Where the content includes any translated material, BMJ does not warrant the accuracy and reliability of the translations (including but not limited to local regulations, clinical guidelines, terminology, drug names and drug dosages), and is not responsible for any error and/or omissions arising from translation and adaptation or otherwise.

Open access This is an open access article distributed in accordance with the Creative Commons Attribution Non Commercial (CC BY-NC 4.0) license, which permits others to distribute, remix, adapt, build upon this work non-commercially, and license their derivative works on different terms, provided the original work is

properly cited, appropriate credit is given, any changes made indicated, and the use is non-commercial. See: <http://creativecommons.org/licenses/by-nc/4.0/>.

ORCID iDs

Virginia Mela <http://orcid.org/0000-0001-7702-0972>

Manuel Bernal <http://orcid.org/0000-0003-0412-3035>

REFERENCES

- Gunstad J, Sanborn V, Hawkins M. Cognitive dysfunction is a risk factor for overeating and obesity. *Am Psychol* 2020;75:219–34.
- Ahima RS. Connecting obesity, aging and diabetes. *Nat Med* 2009;15:996–7.
- Saavedra D, Añé-Kouri AL, Barzilai N, et al. Aging and chronic inflammation: highlights from a multidisciplinary workshop. *Immun Ageing* 2023;20:25.
- Chavakis T, Alexaki VI, Ferrante AW Jr. Macrophage function in adipose tissue homeostasis and metabolic inflammation. *Nat Immunol* 2023;24:757–66.
- Joffin N, Gliniak CM, Funcke J-B, et al. Adipose tissue macrophages exert systemic metabolic control by manipulating local iron concentrations. *Nat Metab* 2022;4:1474–94.
- Hildebrandt X, Ibrahim M, Peltzer N. Cell death and inflammation during obesity: “Know my methods, WAT(son)”. *Cell Death Differ* 2023;30:279–92.
- Verboven K, Wouters K, Gaens K, et al. Abdominal subcutaneous and visceral adipocyte size, lipolysis and inflammation relate to insulin resistance in male obese humans. *Sci Rep* 2018;8:4677.
- Lu Y, Jarrahi A, Moore N, et al. Inflammaging, cellular senescence, and cognitive aging after traumatic brain injury. *Neurobiol Dis* 2023;180:106090.
- Prinz M, Tay TL, Wolf Y, et al. Microglia: unique and common features with other tissue macrophages. *Acta Neuropathol* 2014;128:319–31.
- Marschallinger J, Iram T, Zardeneta M, et al. Lipid-droplet-accumulating microglia represent a dysfunctional and proinflammatory state in the aging brain. *Nat Neurosci* 2020;23:194–208.
- Muscogiuri G, Verde L, Sulu C, et al. Mediterranean Diet and Obesity-related Disorders: What is the Evidence? *Curr Obes Rep* 2022;11:287–304.
- Pardina E, Ferrer R, Rossell J, et al. Diabetic and dyslipidaemic morbidly obese exhibit more liver alterations compared with healthy morbidly obese. *BBA Clin* 2016;5:54–65.
- Prince A, Zhang Y, Croniger C, et al. Oxidative metabolism: glucose versus ketones. *Adv Exp Med Biol* 2013;789:323–8.
- Puchalska P, Crawford PA. Multi-dimensional Roles of Ketone Bodies in Fuel Metabolism, Signaling, and Therapeutics. *Cell Metab* 2017;25:262–84.
- Jin L-W, Di Lucente J, Ruiz Mendiola U, et al. The ketone body β -hydroxybutyrate shifts microglial metabolism and suppresses amyloid- β oligomer-induced inflammation in human microglia. *FASEB J* 2023;37:e23261.
- Shippy DC, Wilhelm C, Viharkumar PA, et al. β -Hydroxybutyrate inhibits inflammasome activation to attenuate Alzheimer’s disease pathology. *J Neuroinflammation* 2020;17:1–12.
- Crawford PA, Crowley JR, Sambandam N, et al. Regulation of myocardial ketone body metabolism by the gut microbiota during nutrient deprivation. *Proc Natl Acad Sci USA* 2009;106:11276–81.
- Gutiérrez-Repiso C, Hernández-García C, García-Almeida JM, et al. Effect of Synbiotic Supplementation in a Very-Low-Calorie Ketogenic Diet on Weight Loss Achievement and Gut Microbiota: A Randomized Controlled Pilot Study. *Mol Nutr Food Res* 2019;63:e1900167.
- Leigh SJ, Morris MJ. Diet, inflammation and the gut microbiome: Mechanisms for obesity-associated cognitive impairment. *Biochim Biophys Acta Mol Basis Dis* 2020;1866:165767.
- Ye YC, Chai SF, Li XR, et al. Intermittent fasting and Alzheimer’s disease-Targeting ketone bodies as a potential strategy for brain energy rescue. *Metab Brain Dis* 2024;39:129–46.
- Pan W, Zhao J, Wu J, et al. Dimethyl itaconate ameliorates cognitive impairment induced by a high-fat diet via the gut-brain axis in mice. *Microbiome* 2023;11.
- Rhea EM, Salameh TS, Logsdon AF, et al. Blood-Brain Barriers in Obesity. *AAPS J* 2017;19:921–30.
- Umpierre AD, Wu LJ. How microglia sense and regulate neuronal activity. *Glia* 2021;93:1637–53.
- Arnoriaga-Rodríguez M, Mayneris-Pexachs J, Burokas A, et al. Obesity Impairs Short-Term and Working Memory through Gut Microbial Metabolism of Aromatic Amino Acids. *Cell Metab* 2020;32:548–60.
- Quek H, Cuni-López C, Stewart R, et al. A robust approach to differentiate human monocyte-derived microglia from peripheral blood mononuclear cells. *STAR Protoc* 2022;3.
- Ferrere G, Tidjani Alou M, Liu P, et al. Ketogenic diet and ketone bodies enhance the anticancer effects of PD-1 blockade. *JCI Insight* 2021;6:e145207.
- Caminhotto R de O, Komino ACM, de Fatima Silva F, et al. Oral β -hydroxybutyrate increases ketonemia, decreases visceral adipocyte volume and improves serum lipid profile in Wistar rats. *Nutr Metab (Lond)* 2017;14:1–9.
- Bolyen E, Rideout JR, Dillon MR, et al. Reproducible, interactive, scalable and extensible microbiome data science using QIIME 2. *Nat Biotechnol* 2019;37:852–7.
- Provencher SW. Estimation of metabolite concentrations from localized in vivo proton NMR spectra. *Magn Reson Med* 1993;30:672–9.
- Righi V, Roda JM, Paz J, et al. 1H HR-MAS and genomic analysis of human tumor biopsies discriminate between high and low grade astrocytomas. *NMR Biomed* 2009;22:629–37.
- Mela V, Mota BC, Milner M, et al. Exercise-induced re-programming of age-related metabolic changes in microglia is accompanied by a reduction in senescent cells. *Brain Behav Immun* 2020;87:413–28.
- Guillot-Sestier M-V, Araiz AR, Mela V, et al. Microglial metabolism is a pivotal factor in sexual dimorphism in Alzheimer’s disease. *Commun Biol* 2021;4:711.
- Holland R, McIntosh AL, Finucane OM, et al. Inflammatory microglia are glycolytic and iron retentive and typify the microglia in APP/PS1 mice. *Brain Behav Immun* 2018;68:183–96.
- Kirmse K, Witte OW, Holthoff K. GABA depolarizes immature neocortical neurons in the presence of the ketone body β -hydroxybutyrate. *J Neurosci* 2010;30:16002–7.
- Lund TM, Obel LF, Risa Ø, et al. β -Hydroxybutyrate is the preferred substrate for GABA and glutamate synthesis while glucose is indispensable during depolarization in cultured GABAergic neurons. *Neurochem Int* 2011;59:309–18.
- Qiao Y-N, Li L, Hu S-H, et al. Ketogenic diet-produced β -hydroxybutyric acid accumulates brain GABA and increases GABA/glutamate ratio to inhibit epilepsy. *Cell Discov* 2023;10:1–20.
- Sae-jie W, Supasai S, Kivimaki M, et al. Triangulating evidence from observational and Mendelian randomization studies of ketone bodies for cognitive performance. *BMC Med* 2023;21:1–10.
- Goldberg EL, Asher JL, Molony RD, et al. β -Hydroxybutyrate Deactivates Neutrophil NLRP3 Inflammasome to Relieve Gout Flares. *Cell Rep* 2017;18:2077–87.
- Youm Y-H, Nguyen KY, Grant RW, et al. The ketone metabolite β -hydroxybutyrate blocks NLRP3 inflammasome-mediated inflammatory disease. *Nat Med* 2015;21:263–9.
- Yamanashi T, Iwata M, Shibushita M, et al. Beta-hydroxybutyrate, an endogenous NLRP3 inflammasome inhibitor, attenuates anxiety-related behavior in a rodent post-traumatic stress disorder model. *Sci Rep* 2020;10:21629.
- Kolb H, Kempf K, Röhling M, et al. Ketone bodies: from enemy to friend and guardian angel. *BMC Med* 2021;19:313.
- Michell-Robinson MA, Touil H, Healy LM, et al. Roles of microglia in brain development, tissue maintenance and repair. *Brain (Bacau)* 2015;138:1138–59.
- Navabi SP, Badreh F, Khombi Shoostari M, et al. Microglia-induced neuroinflammation in hippocampal neurogenesis following traumatic brain injury. *Heliyon* 2024;10:e35869.
- Zhou R, Qian S, Cho WCS, et al. Microbiota-microglia connections in age-related cognition decline. *Aging Cell* 2022;21:e13599.
- Zatcepin A, Gröblich J, Rauchmann BS, et al. Regional desynchronization of microglial activity is associated with cognitive decline in Alzheimer’s disease. *Mol Neurodegener* 2024;19:1–25.
- Aron-Wisniewsky J, Prifti E, Belda E, et al. Major microbiota dysbiosis in severe obesity: fate after bariatric surgery. *Gut* 2019;68:70–82.
- Parhizkar S, Arzberger T, Brendel M, et al. Loss of TREM2 function increases amyloid seeding but reduces plaque-associated ApoE. *Nat Neurosci* 2019;22:191–204.
- Wang Y, Cella M, Mallinson K, et al. TREM2 lipid sensing sustains the microglial response in an Alzheimer’s disease model. *Cell* 2015;160:1061–71.
- Jonsson T, Stefansson H, Steinberg S, et al. Variant of TREM2 associated with the risk of Alzheimer’s disease. *N Engl J Med* 2013;368:107–16.
- Guerreiro R, Wojtas A, Bras J, et al. TREM2 variants in Alzheimer’s disease. *N Engl J Med* 2013;368:117–27.
- Newell C, Bomhof MR, Reimer RA, et al. Ketogenic diet modifies the gut microbiota in a murine model of autism spectrum disorder. *Mol Autism* 2016;7:37.
- Kim M-H, Yun KE, Kim J, et al. Gut microbiota and metabolic health among overweight and obese individuals. *Sci Rep* 2020;10:19417.
- Alexander M, Upadhyay V, Rock R, et al. A diet-dependent host metabolite shapes the gut microbiota to protect from autoimmunity. *bioRxiv* 2024.
- Olson CA, Lum GR, Hsiao EY. Ketone Bodies Exert Ester-Ordinary Suppression of Bifidobacteria and Th17 Cells. *Cell Metab* 2020;31:1049–51.
- Ang QY, Alexander M, Newman JC, et al. Ketogenic Diets Alter the Gut Microbiome Resulting in Decreased Intestinal Th17 Cells. *Cell* 2020;181:1263–75.
- Mardinoglu A, Wu H, Bjornson E, et al. An Integrated Understanding of the Rapid Metabolic Benefits of a Carbohydrate-Restricted Diet on Hepatic Steatosis in Humans. *Cell Metab* 2018;27:559–71.
- Olson CA, Iñiguez AJ, Yang GE, et al. Alterations in the gut microbiota contribute to cognitive impairment induced by the ketogenic diet and hypoxia. *Cell Host Microbe* 2021;29:1378–92.
- Liang X, Fu Y, ting CW, et al. Gut microbiome, cognitive function and brain structure: a multi-omics integration analysis. *Transl Neurodegener* 2022;11:1–14.
- Kang EJ, Cha M-G, Kwon G-H, et al. Akkermansia muciniphila improve cognitive dysfunction by regulating BDNF and serotonin pathway in gut-liver-brain axis. *Microbiome* 2024;12:181.
- Hu N, Pan D, Yang Y, et al. Effects of common plastic products heat exposure on cognition: Mediated by gut microbiota. *Ecotoxicol Environ Saf* 2023;254:114758.

- 61 Liu J, Ye T, Zhang Y, *et al.* Protective Effect of Ginkgolide B against Cognitive Impairment in Mice via Regulation of Gut Microbiota. *J Agric Food Chem* 2021;69:12230–40.
- 62 Morais LH, Schreiber HL, Mazmanian SK. The gut microbiota-brain axis in behaviour and brain disorders. *Nat Rev Microbiol* 2021;19:241–55.
- 63 Bravo JA, Forsythe P, Chew MV, *et al.* Ingestion of Lactobacillus strain regulates emotional behavior and central GABA receptor expression in a mouse via the vagus nerve. *Proc Natl Acad Sci U S A* 2011;108:16050–5.
- 64 Teng Y, Mu J, Xu F, *et al.* Gut bacterial isoamylamine promotes age-related cognitive dysfunction by promoting microglial cell death. *Cell Host Microbe* 2022;30:944–60.
- 65 Mazur-Bialy AI, Pocheć E. Vitamin B2 deficiency enhances the pro-inflammatory activity of adipocyte, consequences for insulin resistance and metabolic syndrome development. *Life Sci* 2017;178:9–16.
- 66 Ahn H, Lee GS. Riboflavin, vitamin B2, attenuates NLRP3, NLRC4, AIM2, and non-canonical inflammasomes by the inhibition of caspase-1 activity. *Sci Rep* 2020;10:19091:19091:.
- 67 Zhang M, Chen H, Zhang W, *et al.* Biomimetic Remodeling of Microglial Riboflavin Metabolism Ameliorates Cognitive Impairment by Modulating Neuroinflammation. *Adv Sci (Weinh)* 2023;10.